Cell surface auxin signalling directly targets PIN-mediated auxin fluxes for adaptive plant development

Lesia Rodriguez[1], Lukáš Fiedler[1], Minxia Zou[1], Caterina Giannini[1], Aline Monzer[1], Zuzana Gelová[1], Inge Verstraeten[1], Jakub Hajný[1,2], Shutang Tan[1], Lukas Hoermayer[1], Lanxin Li[1], Maria Mar Marques-Bueno[3,5], Gergely Molnár[1], Tongda Xu[4], Ivan Kulich[1], Yvon Jaillais[3] and Jiří Friml[1*]

[1]Institute of Science and Technology Austria (ISTA), Am Campus 1, 3400, Klosterneuburg, Austria

[2]Laboratory of Growth Regulators, The Czech Academy of Sciences, Institute of Experimental Botany & Palacký University, Šlechtitelů 27, CZ-78371 Olomouc, Czech Republic

[3]Laboratoire Reproduction et Développement des Plantes Université de Lyon, ENS de Lyon, UCB Lyon 1, CNRS, INRA, F-69342 Lyon, France

[4]Plant Synthetic Biology Center, Haixia Institute of Science and Technology, and College of Life Sciences, Fujian Agriculture and Forestry University, Fuzhou, Fujian, P.R.China

[5]Present Address: Center for Research in Agricultural Genomics (CRAG) CSIC-IRTA-UAB-UB, Barcelona 01893, Spain

* Corresponding author: jiri.friml@ista.ac.at

Lead Contact: Further information and requests for resources and reagents should be directed to and will be fulfilled by the lead contact, Jiří Friml (jiri.friml@ista.ac.at).

SUMMARY

The plant hormone auxin and its directional transport across tissues mediate much of the remarkably adaptive and plastic development of higher plants. Positive feedback between auxin signalling and transport is a key prerequisite for self-organizing development including flexible vascular tissue formation and directional growth responses, such as gravitropism. Here we identified a mechanistic link between cell surface ABP1-based auxin perception, the associated TMK1 kinase and PIN auxin transporters. *abp1* and *tmk1* mutants are defective in auxin-triggered phosphorylation of PIN proteins and in PIN-mediated directional auxin transport. Auxin, via ABP1, induces activation and stabilization of TMK1, thus promoting direct interaction with and phosphorylation of PIN2. Following gravistimulation, the auxin-activated TMK1 acts along the lower root side to reinforce asymmetry in PIN2-mediated auxin fluxes for gravitropic root bending. This ABP1-TMK1-dependent positive feedback on PIN-mediated directional auxin transport is fundamental for robust root gravitropism and presumably also for other self-organizing developmental processes.

KEY WORDS

Auxin, auxin transport, auxin canalization, ABP1, TMK1, protein phosphorylation, root gravitropism

INTRODUCTION

Being sedentary, plants utilize directional growth to spread and position themselves in various environments. Such plant 'movements' according to gravity, light, water availability and other factors are a crucial part of their survival strategy[1]. Other spectacular examples of the superior adaptability of plant development are self-organizing processes such as the formation of an embryonal axis, the regular arrangement of leaves and flowers, the formation of intricate leaf vein patterns, and flexible regeneration of vasculature around a wound. The phytohormone auxin serves as the major endogenous signal behind all this impressive adaptive development[2]. It translates environmental stimuli such as light and gravity into growth responses and aids self-organizing development on account of a feedback regulation between auxin signalling and polar auxin flow[3,4,5].

Directional cell-to-cell auxin transport is a unique, plant-specific mechanism[6] that relies on several plasma membrane-localized transporters[7,8]. Chief among these are the AUX1/LAX auxin importers[9] and the PIN auxin exporters, with the latter determining auxin flow direction by their polarized subcellular localization[10,11]. Inside the cell, auxin triggers a well-studied, predominantly nuclear signalling pathway dependent on TIR1/AFB auxin receptors leading to developmental reprogramming[12,13] and growth regulation[14]. The less well characterized, cell surface auxin signalling involves the AUXIN BINDING PROTEIN 1 (ABP1) receptor and the leucine-rich repeat receptor-like kinase (LRR RLK) TRANSMEMBRANE RECEPTOR-LIKE KINASEs (TMKs)[15,16]. Both these signalling mechanisms are required for auxin feedback on PIN-mediated auxin transport as manifested during the so-called 'auxin canalization', the formation of polarized auxin-transporting channels from a local auxin source[15,17]. Auxin canalization is a process relying on a positive feedback between auxin signalling and auxin transport[3]. This is consistent with theoretical models of auxin feedback-based PIN polarization encompassing both intracellular and cell surface auxin signalling[18]. It has been speculated that auxin impacts PIN activity and polarity by affecting endocytic trafficking[19] involving clathrin-mediated PIN endocytosis[20] and ARF-GEF GNOM-dependent PIN endosomal recycling[21,22] as well as post-translational modifications, chiefly reversible phosphorylation[23,24,25,26]. Nonetheless, the mechanistic link between auxin signalling and PIN-mediated transport has remained elusive.

Fast root gravitropism, mediated by directional auxin flow from the site of gravity perception at the root cap towards the elongation zone where the growth response takes place, is among the latest evolutionary innovations in the quest of plants to grow upright[27]. Besides being a fascinating example of adaptive plant development[28], it is also a perfect model for studying the coordination of auxin signalling and transport. After gravity sensing by sedimenting statoliths in root cap cells[29], the auxin flux is redirected towards the lower side of the root by PIN polarization to bottom cell sides[30,31]. This initial auxin asymmetry is propagated from the root tip to the elongation zone by AUX1- and PIN2-mediated transport[32,33,27], and translated into growth redirection through inhibition of cell elongation at the lower root side[34]. During this response, PIN2 distribution also becomes asymmetric with PIN2 being more

abundant at the lower side of the root as compared to the upper side[35,36]. Such asymmetric PIN2 distribution thus not only propagates, but also reinforces the initial auxin gradient at the root tip, crucially contributing to the robustness of the root bending response as well as to the fine-tuning of gravitropism by other hormonal cues[37]. Nonetheless, the underlying mechanism of this auxin flow reinforcement remains unclear.

Here we uncovered a role of the ABP1-TMK1 cell surface auxin signalling in direct phosphorylation and regulation of PIN auxin transporters. In the context of gravitropic root bending, TMK1 interacts in an auxin-dependent manner with PIN2 and phosphorylates it. This provides a direct mechanism for feedback regulation of auxin transport, applicable not only to gravitropism but also to other developmental processes.

RESULTS

ABP1-TMK1 auxin perception mediates auxin-triggered PIN phosphorylation

ABP1-TMK-mediated cell surface auxin signalling was recently implicated in self-organizing aspects of plant development such as vasculature regeneration and *de novo* establishment of auxin-transporting channels[15]. These phenomena are encompassed by the broader term 'auxin canalization' and are postulated to rely on a direct feedback between auxin signalling and auxin transport[4]. The molecular insights into canalization remained largely enigmatic until the recent identification of CAMEL and CANAR, two LRR RLKs, which target PIN auxin efflux carriers (PINs) to polarize cells for auxin transport across tissues[38].

Motivated by this possible link between phospho-signalling and canalization, we decided to investigate whether auxin perception by ABP1-TMKs might itself feed into PIN-mediated polar auxin transport. We took advantage of a published rapid phospho-proteomic dataset recorded in roots of the *tmk1-1* mutant or WT exactly after 2 minutes of auxin treatment[15,39,40] and examined it for evidence of TMK1-regulated PIN phosphorylation. We identified 12 phospho-sites pertaining to four canonical PINs as putative targets of TMK1 (Figure 1A). Notably, all twelve sites mapped to hydrophilic PIN loops which is the expected location for post-translational modifications regulating PIN polarity and auxin efflux activity[41].

We found two PIN1 phospho-sites (S271, S337), five PIN2 phospho-sites (S179, S183, T233, S393, S439), and two PIN3 phospho-sites (S366, S389) significantly hypo-phosphorylated in the *tmk1-1* mutant compared to WT (Figure 1A). The two PIN1 phospho-sites were previously characterized, PIN1 S271 as a target of the D6PK protein kinase[26] and PIN1 S337 as a target of the MKK7-MPK6 module[42].

117 There were also three hyper-phosphorylated PIN phospho-sites in the *tmk1-1* mutant, one belonging to
118 PIN3 (S294) and two pertaining to PIN7 (S297, S431) (Figure 1A). We next examined the role of ABP1,
119 the auxin receptor upstream of TMK1[15]. We found that eight out of the twelve TMK1-dependent PIN
120 phospho-sites were also significantly hypo-phosphorylated in the *abp1-TD1* mutant compared to WT
121 (Figure 1B).

122 These observations suggest that auxin very rapidly changes the phospho-status of PIN proteins by a
123 mechanism depending on ABP1-TMK1 signalling.

124

125 **ABP1-TMK1 is required for polar auxin transport**

126 We next addressed whether the ABP1-TMK1-mediated PIN phosphorylation has any functional
127 relevance for PIN-mediated polar auxin transport. To this end, we tested basipetal/rootward auxin
128 transport in hypocotyls and basipetal/shootward transport in roots of WT, *abp1*, and *tmk1* mutants.

129 Application of labelled ^{3}H-IAA on decapitated etiolated hypocotyls allows monitoring of the NPA-
130 sensitive[43], mainly PIN1-dependent downward auxin transport[38]. Indeed, *tmk1-1* mutant hypocotyls as
131 well as those of both *abp1* mutant alleles (*abp1-C1* and *abp1-TD1*) showed a decreased rate of ^{3}H-IAA
132 transport (Figure 1C and 1D). Similarly, application of ^{3}H-IAA on the root tip and monitoring of
133 predominantly PIN2-mediated upward auxin transport revealed that the *tmk1-1* and *abp1* mutant roots
134 show a decreased ^{3}H-IAA transport relative to WT (Figure 1E). Importantly, these defects are
135 complemented in the *TMK1::TMK1-FLAG/tmk1-1* (*comp-tmk1-1*) and *ABP1::GFP-ABP1/abp1-C1*
136 (*comp-C1*) lines (Figure 1F).

137 Collectively, this shows that deregulated PIN phosphorylation in *abp1* and *tmk1* mutants correlates with
138 impaired PIN-mediated polar auxin transport in shoots and roots.

139

140 **ABP1 mediates auxin-induced activation of TMK1 in roots**

141 The action of ABP1 as an auxin receptor, auxin-induced ABP1-TMK1 interaction, and similar
142 developmental and cellular phenotypes of the corresponding mutants[15,16], suggest that the ABP1 receptor
143 mediates activation of the TMK1 pathway by auxin. This has been also suggested by previous studies,
144 where auxin stimulates TMK1-dependent ROP2 and ROP6 signalling[16] and TMK1 nanoclustering[44] in
145 pavement cells and MEMBRANE ASSOCIATED KINASE REGULATOR2 (MAKR2) membrane
146 dissociation during root gravitropism[45].

147 TMKs form a redundant family of 4 LRR-RLKs, for which single mutants have only subtle phenotypes,
148 while higher-order mutants show strong defects in many developmental processes[46]. To focus on TMKs
149 in roots we used available global transcriptomic data (Figure S1A and S1B) and generated *TMK1::GUS*,

150 *TMK2::GUS*, *TMK3::GUS* and *TMK4::GUS* lines reporting the corresponding promoter activities. This
151 revealed that TMK1 is the dominant family member highly expressed in roots, followed by TMK3 and
152 TMK4 with lower expression levels (Figure S1C).

153 As an indirect proxy for TMK1 activation in roots we examined the membrane association of ROP6,
154 which has been shown to act downstream of TMK1[16]. Immunoblotting microsomal root protein extracts
155 from auxin-treated (IAA, 5 nM, 0–120 minutes) plants with an anti-ROP6 antibody revealed auxin-
156 induced membrane association of ROP6. This effect was abolished in *tmk1-1* mutant roots (Figure 2A
157 and S2E), confirming that ROP6 activation by auxin is TMK1-dependent.

158 To further confirm these observations and test ABP1 involvement in this process, we detected TMK1-
159 mediated activation of ROP signalling using an orthogonal method. As usual for small GTPases, only
160 GTP-bound (active) but not GDP-bound (inactive) ROP proteins engage in protein-protein interactions
161 with their effectors. We purified the Cdc42/Rac interactive binding motif (CRIB) domain of the RIC1
162 ROP effector from bacteria and used it to pull down active ROPs from root protein extracts.
163 Immunoblotting with an anti-ROP2 antibody revealed auxin-induced (IAA, 100 nM, 10 minutes) ROP2
164 activation in WT but not in *tmk1-1* roots and importantly neither in *abp1-C1* or *abp1-TD1* roots (Figure
165 2B). These results demonstrate that in roots auxin triggers ROP2 and ROP6 signalling downstream of
166 ABP1-TMK1 signalling.

167 Next, we analysed TMK1 phosphorylation in response to auxin. The TMK1 kinase domain is known to
168 be capable of auto-phosphorylation[47], and numerous studies have shown that changes in phosphorylation
169 of the cytoplasmic domain of LRR-RLKs are indicative of LRR-RLK activation in plants[48,49]. Therefore,
170 we examined TMK1 phosphorylation by performing a Phos-tag Biotin Probe binding analysis on
171 TMK1-FLAG immunoprecipitated from auxin-treated (IAA, 10 nM, 1 hour) *TMK1::TMK1-*
172 *FLAG*/*tmk1-1* roots. With this approach, we revealed that auxin induced phosphorylation and therefore
173 activation of TMK1 in roots (Figure 2C and S2C). Unexpectedly, we observed that auxin treatment
174 increased not only the [phospho-TMK1/total TMK] ratio (Figure S2C) but also the total TMK1
175 abundance (Figure 2C). Immunoblotting microsomal root protein extracts from WT (anti-TMK1
176 antibody), *TMK1::TMK1-FLAG* (anti-FLAG antibody), and *UBQ10::TMK1-3xHA* (anti-HA antibody)
177 confirmed auxin-mediated (anti-TMK1: IAA, 5 nM, 0–120 minutes; anti-FLAG/HA: IAA, 5 or 10 or
178 100 nM, 1 hour) increase in TMK1 abundance (Figure 2A, S2A, S2B and S2E). In contrast, *TMK1*
179 mRNA levels as determined by RT-qPCR did not increase but rather decreased with IAA treatment
180 (IAA, 10 or 100 nM, 0–120 minutes: Figure S2D). This suggests that auxin upregulates TMK1
181 abundance on the protein level rather than transcriptionally. We also monitored TMK1-GFP signal after
182 auxin treatment (IAA, 5 or 10 nM, 3.5-hour time course) of *TMK1::TMK1-GFP*/WT roots. In agreement
183 with biochemical data, concentrations as low as 5 nM of IAA led to a strong increase in the TMK1-GFP
184 signal (Figure 2D and 2E).

185 In totality, our experiments in roots suggest that auxin, via ABP1, promotes TMK1 phosphorylation and
186 stabilization at the plasma membrane, underlying TMK1 activation and leading to downstream
187 signalling. This provides a possible mechanism for how auxin could act through the ABP1-TMK1
188 pathway to trigger phosphorylation of PINs and other targets.

189

190 **TMK1 interacts with and phosphorylates PIN2**

191 Given that most TMK1-regulated PIN phospho-sites were identified in PIN2 (Figure 1A) and its
192 prominent role in root gravitropism, we further focused on PIN2 as a representative of PINs.

193 To address whether TMK1 regulates PIN2 directly, we performed a co-immunoprecipitation analysis
194 (Co-IP) between endogenous PIN2 and TMK1. We immunoprecipitated TMK1-FLAG from
195 *TMK1::TMK1-FLAG/tmk1-1* roots and then used an anti-PIN2 antibody for detection of native PIN2.
196 PIN2 did not co-immunoprecipitate with TMK1-FLAG in untreated samples. However, in auxin-treated
197 roots (IAA, 5 or 20 nM, 15 or 30 minutes) we could co-immunoprecipitate PIN2 with TMK1-FLAG
198 and the Co-IP efficiency increased with the duration of IAA treatment (Figure 3A and S3A), suggesting
199 an auxin-dependent interaction of TMK1 with PIN2.

200 To verify the biochemical evidence for TMK1-PIN2 interaction, we employed the quantitative FRET-
201 FLIM technique. We co-expressed *35S::TMK1-GFP* and *35S::PIN2-mCherry* in *Arabidopsis* root
202 protoplasts and measured the fluorescence lifetime of the GFP signal. The lifetime of TMK1-GFP was
203 reduced after co-expression with PIN2-mCherry, which supported the interaction between TMK1 and
204 PIN2 (Figure 3B). The negative controls, an unrelated receptor-like kinase FLS2-GFP and $TMK1^{\Delta KD}$-
205 GFP with a truncated kinase domain, showed a less pronounced decrease in fluorescence lifetime,
206 confirming the specificity of the TMK1-PIN2 interaction (Figure 3B and S3B).

207 Given the direct interaction of TMK1 with PIN2, it seemed likely that at least some of the TMK1-
208 regulated PIN2 phospho-sites (Figure 1A) could be ascribed to direct phosphorylation by TMK1. To
209 test this, we performed an *in vitro* phosphorylation assay with ^{32}P-ATP as a phosphate donor by
210 incubating a purified N-terminal His-tagged hydrophilic loop (HL) of PIN2 with TMK1-3xHA
211 immunoprecipitated from a root protein extract. These *in vitro* assays showed that TMK1-3xHA
212 mediated the phosphorylation of His-PIN2 HL. Notably, only intact TMK1-HA but not the kinase-dead
213 version $TMK1^{K616R}$-HA was able to phosphorylate His-PIN2-HL (Figure 3C). We did not observe any
214 auxin effect in these kinase assays (Figure S3C), but this could be explained if TMK1-3HA activity was
215 already saturated by endogenous auxin during immunoprecipitation from TMK1-3xHA roots.

216 In conclusion, our data demonstrate that the receptor-like kinase TMK1 interacts, in an auxin-dependent
217 manner, with the PIN2 auxin efflux carrier and phosphorylates its hydrophilic loop.

218

219 **TMK1 modulates PIN2 levels during the root response to exogenous auxin**

220 The compromised PIN2-mediated shootward auxin transport in *abp1* and *tmk1* mutant roots (Figure 1)
221 suggested an involvement of ABP1-TMK1 signalling in PIN2 functionality. Therefore, we tested
222 whether TMK1-mediated PIN2 phosphorylation influences its polarity and abundance, both of which
223 are known to be regulated by phosphorylation[41]. We did not observe any obvious changes in PIN2
224 polarity as assessed by anti-PIN2 immunolocalization experiments in *tmk1* mutants (data not shown),
225 thus we examined the effects of auxin on PIN2 levels in WT and *tmk1-1* by immunoblotting microsomal
226 root samples with an anti-PIN2 antibody. In WT, 5 nM IAA stabilized PIN2 over the course of a 1-hour
227 treatment, but after 2 hours PIN2 decreased below starting levels (Figure 4A and S4A). With 10 nM
228 IAA, however, PIN2 was destabilized already after 1 hour (Figure S4B). Such complex PIN2 dynamics
229 in response to short versus long auxin treatments were described before for the synthetic auxin NAA[35,50].
230 Investigation of PIN2 transcription by RT-qPCR confirmed that regulation of PIN2 stability by auxin is
231 independent of transcription (Figure S4C). Thus, auxin initially stabilizes and after a prolonged exposure
232 destabilizes PIN2, consistent with previous reports[19,35].

233 Notably, the *tmk1-1* mutant exhibited premature PIN2 stabilization by IAA and showed resistance to
234 long-term PIN2 downregulation (Figure 4A, S4A and S4B). We further assessed PIN2 abundance in
235 auxin-treated WT and *tmk1-1* roots by live imaging. IAA treatment of PIN2-GFP roots caused a decrease
236 in the GFP signal in a concentration-dependent manner. This auxin effect was not observed or even
237 reverted in the *tmk1-1* mutant (Figure 4b and 4C), overall indicating that TMK1 mediates PIN2
238 destabilization, which is triggered by exogenous auxin.

239

240 **TMK1 kinase activity is required for the root gravitropic response**

241 To test the relevance of our observations on PIN2 regulation by auxin and by TMK1 in a physiological
242 context, we focused on gravitropism, a classic developmental process during which membrane PIN2
243 levels undergo dynamic spatiotemporal changes[35,36], and which has been proposed to be regulated by
244 TMK1 and its inhibitory protein MAKR2[45]. Analysis of root growth in verified *tmk* single mutants
245 (Figure S5A) did not show obvious defects in growth rate (Figure S5C), but time-lapse imaging of root
246 bending following gravistimulation revealed slower gravitropic response kinetics compared to WT
247 plants. This defect was most pronounced in the *tmk1-1* mutant and complemented in the *TMK1::TMK1-*
248 *FLAG/tmk1-1* line (Figure 5A and 5B; Figure S5B and S5C; Table S1 and S2). *tmk4-1* roots also bent
249 less efficiently; *tmk3-1* had a very weak defect, whereas *tmk2-1* showed normal gravitropic bending
250 (Figure S5B and S5C; Table S2), which is consistent with the very low expression of *TMK2* in the root
251 (Figure S1A, S1B and S1C). Notably, the kinase activity of TMK1 is required for its role in root

252 gravitropism since the expression of TMK1 without a kinase domain (*35S::TMK1$^{\Delta KD}$-GFP*) or TMK1
253 carrying a mutation in the ATP-binding site (*UBQ10::TMK1^{K616R}-mCherry*) also conveyed defects in
254 root gravitropism, even when introduced into WT plants (Figure 5A and 5B; Figure S5D and S5E; Table
255 S2). Of note, the two kinase-dead lines showed fluorescent signal distribution comparable to that of
256 *TMK1::TMK1-GFP* (Figure S1D and S5F).

257 Next, we tested whether TMK1 is involved in gravity-induced auxin re-distribution by introducing the
258 *DR5rev::GFP* auxin response reporter into the *tmk1-1* loss-of-function mutant. Monitoring the DR5
259 signal following gravistimulation showed significantly less auxin response asymmetry in the *tmk1-1*
260 mutant as compared to WT control (Figure 5C and 5D).

261 These results show that, during root gravitropism, TMK1 is involved in both the asymmetric distribution
262 of auxin and in root bending.

263

264 **TMK1 mediates PIN2 asymmetry during root gravitropic response**

265 Having confirmed that TMK1 signalling is required for the root gravitropic response and given that
266 TMK1 mediates PIN2 phosphorylation (Figure 1A and 3C) and stability (Figure 4), we examined the
267 dynamic regulation of PIN2 abundance in response to gravity by immunoblotting microsomal root
268 protein extracts. After 1 hour of gravistimulation, WT roots showed modest PIN2 stabilization; this was
269 followed by a decrease below starting levels at the 2-hours timepoint without further changes for the
270 rest of the time course (Figure 6A and S6C). The *tmk1-1* mutant PIN2 levels, however, increased
271 dramatically after 1 hour of gravistimulation and then slowly recovered back to the starting value after
272 4 hours of gravistimulation. This biochemical evidence reveals dynamic regulation of total PIN2
273 abundance during gravitropism, which is mediated by TMK1.

274 To gain more spatial insights into the behaviour of PIN2 during the gravity response, we performed live
275 imaging and followed PIN2-GFP asymmetry in WT and *tmk1-1* roots after gravistimulation. While WT
276 roots established asymmetric PIN2 distribution as expected, this response was abrogated in the *tmk1-1*
277 mutant (Figure 6C and 6D). Importantly, the *tmk1-1* mutant showed defects in both PIN2 stabilization
278 at the lower side of the root (from 2 hours onwards) and in the destabilization of PIN2 at the upper side
279 of the root (the 3 hours timepoint) (Figure 6D).

280 Thus, TMK1 orchestrates a complex, dynamic regulation of PIN2 abundance during gravitropism which
281 provides a likely explanation for the gravitropic phenotype of the *tmk1* mutant.

282

283 **TMK1 activity and asymmetric abundance during root gravitropism**

284 The gravitropic phenotype of *tmk1-1* roots suggested to us that TMK1 might become activated during
285 the root gravitropic response. Immunoblotting WT root microsomal fractions from gravistimulated
286 seedlings with an anti-ROP6 antibody confirmed that gravistimulation activated ROP6 signalling. The
287 absence of these dynamics in the *tmk1-1* mutant showed that gravity-induced ROP6 activation was
288 TMK1-dependent (Figure 6A and S6C). We subsequently conducted a Phos-tag Biotin Probe binding
289 analysis on TMK1-FLAG immunoprecipitated from gravistimulated *TMK1::TMK1-FLAG/tmk1-1*
290 roots. This revealed a significant increase in TMK1 phosphorylation already after 1 hour of
291 gravistimulation (Figure 6B and S6D) demonstrating that gravistimulation activates TMK1. Similar to
292 our experiments with a time course of exogenous auxin (Figure 2A and 2C), we noted an increase in
293 TMK1 abundance over the course of gravistimulation (Figure 6B). Increasing TMK1 levels were also
294 apparent from Western blots performed on microsomal root extracts from gravistimulated seedlings
295 (Figure 6A; Figure S6A, S6B and S6C). Collectively, these data show that gravistimulation activates
296 TMK1 signalling in roots by impacting both the TMK1 phosphorylation status and stability.

297 To gain additional spatial information on this regulation, we performed live imaging on the
298 *TMK1::TMK1-GFP* line. Strikingly, we observed that after 1 hour of gravistimulation TMK1-GFP
299 developed an asymmetric pattern with higher signal intensity along the lower root side, which was
300 getting more pronounced over time (Figure 6E and 6F). This result is consistent with auxin accumulating
301 at the lower root side stabilizing TMK1 as seen for exogenous auxin application (Figure 2D and 2E).
302 This implies the existence of additional signals/regulations at the lower side of the root during the
303 graviresponse or some compensatory mechanism in the *tmk1-1* mutant, which causes bulk stabilization
304 of PIN2 and overshadows the fact that, in WT roots, the function of TMK1 is to stabilize PIN2 at the
305 lower root side shortly after gravistimulation. It is tempting to propose a model in which TMK1
306 stabilization at the lower root side reinforces PIN2 asymmetry to confer robustness on root gravitropism
307 in land plants, however, it remains a challenge for future studies to fully consolidate all the above-
308 mentioned intriguing observations.

309 Nonetheless, our data reveal crucial importance of TMK1 for dynamic PIN2-mediated fluxes and auxin
310 asymmetry in driving root gravitropism. Notably, auxin-triggered TMK1-PIN2 interaction and
311 phosphorylation provides a plausible mechanism for how this regulation occurs.

312

313 **DISCUSSION**

314

315 **ABP1 relays auxin signal for TMK1 activation and stabilization**

316 Cell surface auxin signalling, unlike the TIR1/AFB transcriptional pathway based predominantly in the
317 nucleus[51], has been a matter of considerable controversy[52]. Only recently was it confirmed in
318 *Arabidopsis* that ABP1 acts as an apoplastic auxin-binding receptor[15], which associates to the

319 extracellular domain of TMK1[16]. This provides a plausible mechanism for how extracellular auxin can
320 induce via ABP1 the phosphorylation of proteins in the cell interior, either directly through the cytosolic
321 kinase domain of TMK1 or through downstream kinase cascades. Indeed, *abp1* and *tmk1* mutants show
322 aberrant and highly inter-correlated phospho-proteomes[15,39]. Overall, the auxin-induced ABP1-TMK1
323 association[16], failure of *abp1* mutants to maintain steady-state TMK phosphorylation[15], and the lack of
324 ROP signalling downstream of TMK1 in response to auxin (Figure 2B and [16]) strongly support the notion
325 that ABP1 acts as a receptor communicating auxin for TMK-mediated phosphorylation.

326 It comes as a surprise that auxin not only induces TMK1 phosphorylation but also its persistent
327 stabilization. This is to be contrasted with the usual textbook signalling paradigm where prolonged
328 stimulation desensitizes the pathway in question. For instance, mammalian receptor tyrosine kinases
329 such as the EPIDERMAL GROWTH FACTOR RECEPTOR (EGFR) are endocytosed and almost
330 completely degraded within 1-2 hours of ligand application[53,54]. This peculiar TMK1 behaviour may
331 constitute a part of the positive feedback linking auxin to its transport that has been proposed as a central
332 mechanism behind canalization-mediated self-organized plant development[3]. It is conceivable that
333 canalization would rely on a positive feedback loop which persists until the process is completed rather
334 than on rapid desensitization. Furthermore, extracellular auxin perception has been predicted as a key
335 signalling input parameter for auxin canalization[18]. Consistent with these notions, auxin canalization
336 and canalization-mediated vascular tissue regeneration are severely defective in *abp1* and *tmk* mutants[15].
337 Despite these strong, specific defects, overall growth and development is not strongly affected following
338 single-gene lesions within the ABP1-TMK pathway, which can be explained by the genetic redundancy
339 between TMKs[46] and between ABP1 and its homologues[55]. Thus, ABP1-TMK cell surface signalling is
340 a likely input component of the positive feedback central to the auxin canalization mechanism.
341

342 **Auxin induced TMK1-PIN2 interaction and phosphorylation for PIN2 stability**

343 The biological roles of the global, ultrafast phosphorylation downstream of ABP1-TMK1 remain
344 unclear but prominent among the phosphorylated targets are multiple PIN auxin transporters (Figure
345 1A, 1B and [39]). The activity, stability and polar localization of PINs are known to be regulated heavily
346 by complex phosphorylation on multiple sites by different types of kinases in response to various
347 signals[41]. Accordingly, PIN-mediated auxin transport in shoots and roots of *abp1* and *tmk1* mutants is
348 compromised (Figure 1C-F) implying that PIN regulation by ABP1-TMK1 is functionally relevant.

349 It appears clear that ABP1 transmits the auxin signal to TMKs for their phosphorylation and activation,
350 thus enabling the phosphorylation of downstream targets such as PINs. What part of the phosphorylation
351 response emanating from ABP1-TMK1 is attributable to direct TMK1 action on substrate proteins,
352 however, remains elusive. At least in the case of PINs, as exemplified by PIN1[56] and PIN2 (Figure 3),
353 TMK1 engages in a direct interaction and in an auxin-dependent manner phosphorylates multiple
354 residues within their hydrophilic loops. While for PIN1 the phosphorylation seems relevant to its polar

355 localization in tissues[56], PIN2 undergoes dynamic stabilization and destabilization in response to the
356 TMK1-transduced auxin phospho-signalling. The former scenario is likely relevant to classical auxin
357 canalization, the latter for fine-tuning of auxin fluxes during root gravitropism. Thus, distinct PINs
358 phosphorylated by TMK1 at different residues can be regulated by auxin in ways depending on the
359 developmental context. Regardless of specifics of the regulation, the auxin input via ABP1-TMK1 and
360 its direct modulation of PIN activity represent a core mechanism for the positive feedback between auxin
361 signalling and directional transport.
362
363 **TMK1-PIN2 module during root gravitropism**
364 PIN2 evolved as a specific component of efficient root gravitropism of seed plants, which contributed
365 to their successful colonization of land habitats[27]. The key evolutionary innovation has been the
366 directional, PIN2-mediated auxin flow that carries the signal from the site of gravity perception at the
367 root tip to the site of growth response in the elongation zone[28]. Notably, PIN2 abundance also becomes
368 asymmetric with more PIN2 at the lower root side[35,36], which reinforces the initial auxin gradient and
369 contributes to the robustness of the root bending response[37]. This provides an excellent model to study
370 the interplay of auxin signalling and transport. TMK1 is required for the full extent of asymmetric auxin
371 distribution and for root bending during the gravitropic response. This is elegantly explained by the fact
372 that *tmk1* roots cannot establish asymmetric PIN2 distribution during the graviresponse (Figure 6C, 6D
373 and [57]). TMK1 protein abundance increases dynamically during root gravitropism along the lower side
374 of the root, mirroring the asymmetric auxin distribution and PIN2 accumulation.

375 The above observations lead to a model in which the initial auxin flow asymmetry following
376 gravistimulation activates and stabilizes TMK1 at the lower root side and promotes its interaction with
377 PIN2, leading to PIN2 phosphorylation. This positive feedback loop between auxin and PIN2-mediated
378 transport reinforces the auxin flow at the lower root side and contributes to a robust gravitropic response.
379 However, TMK1-mediated persistent PIN2 destabilization in response to exogenous auxin treatment
380 (Figure 4) is not consistent with PIN2 stabilization at the place of elevated auxin along the lower side of
381 the gravistimulated root, indicating a possible hidden complexity and variables. Regardless of these
382 additional regulations, the asymmetric action of TMK1 following gravistimulation and the TMK1-PIN2
383 feedback loop clearly are required for PIN2 asymmetry during gravitropism, and consequently for a
384 robust bending response.
385
386 **Conclusions**
387 Here we identified a mechanism for the positive feedback between auxin and its transport, which is a
388 key prerequisite for canalization-guided plant development. It involves auxin-triggered phosphorylation
389 of multiple PIN auxin transporters. Exemplified by PIN2, this regulation involves a direct interaction
390 with the TMK1 receptor-like kinase. The input for TMK1 activation comes from auxin binding to the

ABP1 receptor at the cell surface, resulting in TMK1 phosphorylation, long-term TMK1 stabilization at the plasma membrane, and activation of downstream processes. This positive feedback regulation is required in the case of PIN2 for robust asymmetric auxin fluxes during root gravitropism and in the case of PIN1[56] most likely for auxin canalization-mediated flexible vascular tissue formation and regeneration. Thus, TMK-based auxin feedback regulation may represent a more general mechanism acting in different developmental contexts with different PIN transporters, thereby mediating specialized aspects of adaptive and self-organized development in plants. It is remarkable that the herein identified auxin feedback on its transport via TMK-based cell surface signalling likely evolved from an ancestral and ancient phosphorylation response to the small molecule auxin[39,40], later diversifying to guide the complex and flexible auxin-regulated development of morphologically complex land plants.

ACKNOWLEDGEMENTS

We thank W. Gray for providing material, N. Gnyliukh and E. Cervenova for help with manuscript preparation. To Dolf Weijers and Mark Roosjen, we thank for encouraging discussions and support with phospho-proteomic analyses. We thank Bioimaging and Life Science facilities at IST Austria for an excellent service and assistance. The research leading to these results has received funding from the European Research Council (ERC) under the European Union's Horizon 2020 research and innovation programme grant agreement No 742985 and Austrian Science Fund (FWF): I3630-775 B25 to J.F; National Natural Science Foundation of China (Grant 32130010, 31422008), start-up funds from FAFU to T.X.. Y.J. was funded by ERC no. 3363360-APPL under FP/2007-2013. L.R. was supported by FP7-PEOPLE-2011-COFUND ISTFELLOW program (IC1023FELL01) and the European Molecular Biology Organization (EMBO) long-term postdoctoral fellowship (ALTF 985-2016).

AUTHOR CONTRIBUTIONS

Conceptualization: J.F., L.R.; Methodology: L.R., I.K.; Investigation: L.R., L.F., M.Z., C.G., A.M., Z.G., I.V., J.H., M.R., S.T., G.M., L.H., L.L.; Resources: L.R., M.M.M.-B, Y.J., T.X.; Writing: J.F., L.F., L.R.; Review & Editing: all authors; Visualization: L.R., L.F.; Supervision: L.R., J.F.; Funding Acquisition: J.F., D.W.

DECLARATION OF INTERESTS

The authors declare no competing interests.

424

425

426 **FIGURE TITLES AND LEGENDS**

427

428 **Figure 1.**

429 **Figure 1. ABP1-TMK1 auxin perception targets PIN phosphorylation and polar auxin transport.**

430 (A) Overview of PIN phospho-sites significantly regulated (FDR < 0.05) in *tmk1-1* mutant roots
431 compared to WT after treatment with auxin (100 nM, 2 min). 4 independent biological replicates, mean
432 ± SD, permutation-based t-tests with FDR-controlled p-values. Highlighted in bold are sites which are
433 co-regulated in the *abp1-TD1* mutant. Data adapted from [15]. *p < 0.05, **p < 0.01, ***p < 0.001, ****p
434 < 0.0001.

435 (B) Overview of PIN phospho-sites significantly regulated (FDR < 0.05) in *abp1-TD1* mutant roots
436 compared to WT after treatment with auxin (100 nM, 2 min). 4 independent biological replicates, mean
437 ± SD, permutation-based t-tests with FDR-controlled p-values. Highlighted in bold are sites which are
438 co-regulated in the *tmk1-1* mutant. Data adapted from [15]. *p < 0.05, **p < 0.01, ***p < 0.001, ****p <
439 0.0001.

440 (C) Basipetal/rootward transport of radioactive ^{3}H-IAA in decapitated hypocotyls is defective in the
441 *tmk1-1* mutant (genotype/treatment fixed effect: χ^2 = 60.64, df = 2, p = 6.78e-14). 10 µM NPA, an
442 inhibitor of auxin transport, was used as a negative control. Pooled data from two independent
443 experiments with similar results (repetition random effect: ΔAIC = 2.0, df = 1, p = 0.9999), mean ± SD.
444 Asterisks show Holm-corrected unpaired two-sided t-tests. *p < 0.05, **p < 0.01, ***p < 0.001, ****p
445 < 0.0001.

446 D) Basipetal/rootward transport of radioactive ^{3}H-IAA in decapitated hypocotyls is defective in *abp1*
447 mutants (one-way ANOVA: $F_{3,8}$ = 60.13, p = 7.86e-06). 10 µM NPA, an inhibitor of auxin transport,
448 was used as a negative control. Single experiment, n = 3 for each condition, mean ± SD. Asterisks show
449 Holm-corrected unpaired two-sided t-tests. *p < 0.05, **p < 0.01, ***p < 0.001, ****p < 0.0001.

450 (E) Basipetal/shootward transport of radioactive ^{3}H-IAA in roots is defective in *tmk1-1* and *abp1*
451 mutants (genotype/treatment fixed effect: χ^2 = 32.30, df = 4, p = 1.66e-06). Pooled data from two
452 independent experiments with similar results (repetition random effect: ΔAIC = 1.1, df = 1, p = 0.0804),
453 mean ± SD. Asterisks show Holm-corrected unpaired two-sided t-tests. *p < 0.05, **p < 0.01, ***p <
454 0.001, ****p < 0.0001.

455 (F) Complementation of defects in root basipetal/shootward transport of radioactive ^{3}H-IAA for the
456 *TMK1::TMK1-FLAG/tmk1-1* (*comp-tmk1-1*) and *ABP1::GFP-ABP1/abp1-C1* (*comp-abp1-C1*) lines.
457 Single experiment, n = 10 for each condition, mean ± SD.

458

459 **Figure 2.**

460 **Figure 2. Auxin-induced activation of cell surface ABP1-TMK1 signalling in roots.**

461 (A) Western Blot: time course of endogenous TMK1 and ROP6 protein levels in the microsomal fraction
462 of 4-day-old WT and *tmk1-1* roots treated with 5 nM IAA (see Figure S2E for quantification). The
463 experiment was repeated 3 times and representative data are shown. The loading control is reused in
464 Figure 4A which depicts more data from the same experiment.

465 (B) Auxin-mediated activation of ROP signalling is defective in *tmk1-1* and *abp1* mutant backgrounds.
466 Pull-down of active ROP GTPases from root protein extracts using a heterologously expressed GST-
467 tagged CRIB domain from the RIC1 ROP effector. Both input and pull-down gels were blotted with an
468 anti-ROP2 antibody.

469 (C) Comparison of TMK1-FLAG phosphorylation in untreated roots and roots treated with 10 nM IAA
470 for 1h. Root *TMK1::TMK1-FLAG/tmk1-1* extracts treated with 10 nM IAA or DMSO control for 1 hour
471 were used for immunoprecipitation with anti-Flag antibody. Phos-tag Biotin Probe was used to analyse
472 TMK1 phosphorylation levels and anti-Flag antibody for total amount of immunoprecipitated TMK1-
473 FLAG (see figure S2C for quantification).

474 (D) Representative intensity-coloured images of *TMK1::TMK1-GFP* expression in 4-day-old seedlings
475 after a 3-hour treatment with 5 or 10 nM IAA. Scale bars represent 20 µm.

476 (E) Time-course quantification of *TMK1::TMK1-GFP* signal in root tips treated with IAA (5 or 10 nM)
477 or DMSO control, normalized to the initial fluorescence value. Mean ± SD (n = 20; experiment repeated
478 3 times with representative data depicted).

479

480 **Figure 3.**

481 **Figure 3. Auxin-mediated TMK1 interaction with and phosphorylation of PIN2.**

482 (A) Auxin promotes the interaction between TMK1 and PIN2 in a co-immunoprecipitation (Co-IP)
483 assay. Microsomal protein fraction from 20 nM IAA- or DMSO-treated roots expressing *TMK1::TMK1-*
484 *FLAG/tmk1-1* was immunoprecipitated with an anti-FLAG antibody, and endogenous PIN2 was
485 detected by blotting with an anti-PIN2 antibody. See Figure S3A for Co-IP with 5 nM IAA where input
486 PIN2 abundance in the protein microsomal fraction is increased.

487 (B) FRET-FLIM analysis on transiently expressed *35S::TMK1-GFP, 35S::TMK1$^{\Delta KD}$-GFP, 35S::FLS2-*
488 *GFP* and *35S::PIN2-mCherry* in root protoplasts. Fluorescence lifetime values are displayed as a heat
489 map (for additional images see Figure S3B). Two-way ANOVA with post hoc tests (*p < 0.05; ****p
490 < 0.0001).

491 (C) *In vitro* kinase assay showing that TMK1-3xHA directly phosphorylates the 6His-PIN2 hydrophilic
492 loop (HL). Top panel, ^{32}P autoradiography; middle panel, CBB staining; bottom panel, immunoblot with
493 an anti-HA antibody.

494

495 **Figure 4.**

496 **Figure 4. TMK1 dynamically regulates root PIN2 levels in response to exogenous auxin.**

497 (A) Western Blot: time course of endogenous PIN2 protein levels in the microsomal fraction of 4-day-
498 old WT and *tmk1-1* roots treated with 5 nM IAA (see Figure S4A for quantification). The experiment
499 was repeated 3 times and representative data are shown. The loading control (reused) and the anti-PIN2
500 immunoblot come from the same experiment as that shown in Figure 2A.

501 (B) Representative intensity coloured images of *PIN2::PIN2-GFP* after a 3-hour treatment with 10 nM
502 IAA. Scale bars, 20 μm.

503 (C) Quantification of *PIN2::PIN2-GFP* in root tips of WT or *tmk1-1* seedlings treated with IAA (5, 10
504 nM or DMSO control), normalized to the initial fluorescence value. Mean ± SD (n = 20; experiment
505 repeated 3 times with representative data depicted).

506

507 **Figure 5.**

508 **Figure 5. TMK1 kinase activity is required for the gravitropic response.**

509 (A) Representative images of root bending 3 hours after a 90° rotation for 4-day-old WT, mutant *tmk1-*
510 *1*, kinase-dead *UBQ10::TMK1^{K616R}-mCherry,* and genetically complemented *TMK1::TMK1-*
511 *FLAG/tmk1-1* seedlings.

512 (B) Time course of the gravitropic response for lines shown in (A) measured every 30 minutes, mean ±
513 SD (n = 10; experiment repeated 3 times, a representative run is depicted). See Figure S5E for complete
514 analysis and root growth rate data, and Table S2 for statistical analysis.

515 (C) Representative confocal images of asymmetric auxin response (visualized by *DR5rev::GFP*) at the
516 lower side of the root before and after a 3-hour gravistimulation in WT and *tmk1-1* 4-day-old roots.

517 (D) Quantification of *DR5rev::GFP* asymmetry as a ratio of fluorescence intensity at the lower side to
518 the upper side of gravistimulated roots at the indicated time points, normalized to the initial fluorescence
519 value. Mean ± SEM of at least 3 independent experiments, n = 10. Two-way ANOVA with Dunnett's
520 multiple comparison tests (*$p < 0.05$, **$p < 0.01$). 'g' represents the gravity vector.

521

522 **Figure 6.**

523 **Figure 6. TMK1 mediates PIN2 asymmetry during the root gravitropic response.**

524 (A) Western Blot: time course of endogenous TMK1, ROP6 and PIN2 protein levels in the microsomal
525 fraction of 4-day-old WT and *tmk1-1* roots after 0, 1, 2, 3 and 4 hours of gravistimulation. The
526 experiment was repeated 3 times and representative data are shown. For quantification of protein levels
527 see Figure S6C.

528 (B) TMK1-FLAG phosphorylation after gravistimulation. *TMK1::TMK1-FLAG/tmk1-1* was
529 immunoprecipitated with an anti-FLAG antibody and detected using a Phos-tag Biotin Probe (see Figure
530 S6D for quantification).

531 (C) Representative images of *PIN2::PIN2-GFP* in 4-day-old WT and *tmk1-1* seedlings after 4 hours of
532 gravistimulation within a time course of 0, 2, 3, 4 and 5 hours of gravistimulation. 'g' represents the
533 gravity vector. Scale bars, 20 µm.

534 (D) Quantification of PIN2-GFP ratio between the lower and upper sides of gravistimulated roots,
535 normalized to the initial fluorescence value at the indicated time point. Mean ± SD (n = 8; experiment
536 repeated 3 times with representative data depicted). Significant differences to timepoint 0 are shown by
537 *p*-values, two-way ANOVA with Dunnett's post hoc tests (**** $p < 0.0001$).

538 (E) Intensity-coloured map of 4-day-old *TMK1::TMK1-GFP* root tips before and after 3 hours of a 90°
539 gravitropic stimulus. White arrows indicate asymmetric TMK1-GFP distribution. Scale bars, 20 µm.

540 (F) Quantification of TMK1-GFP in the epidermis and cortex of the upper and lower root sides
541 normalized to the initial fluorescence value, mean ± SD (n = 10). Experiment repeated 3 times with
542 representative data depicted. Significant differences to timepoint 0 are shown by *p*-values, two-way
543 ANOVA with Dunnett's post hoc tests (**** $p < 0.0001$).

544

545 **Figure S1.**

546 **Figure S1. Expression of the TMK leucine-rich repeat receptor-like (LRR-RLK) kinase family**
547 **in roots.**

548 (A) Relative transcription levels of *TMK1*, *TMK2*, *TMK3* and *TMK4* in *Arabidopsis* roots from 803
549 samples assayed with the Affymetrix Arabidopsis ATH1 Genome Array. Data was obtained from the
550 Genevestigator database (https://genevestigator.com). Mean ± SD.

551 (B) Relative expression levels of *TMK1, TMK2, TMK3* and *TMK4* in different root cell types obtained
552 from high-resolution spatiotemporal microarray analysis of 5–6-day old roots reported in [58] (ePlant
553 http://bar.utoronto.ca/eplant).

554 (C) Root tip expression pattern of *TMK1*, *TMK2*, *TMK3*, and *TMK4* promoters fused to the GUS
555 transcriptional reporter. Scale bars, 100 µm.

556 (D) Representative intensity-colored image of *TMK1::TMK1-GFP* expression in 4-day-old root tips.

557

558 **Figure S2.**

559 **Figure S2. Auxin promotes TMK1 stability, phosphorylation state, and downstream signalling.**

560 (A) Western blotting of total root protein extracts of 4-day-old *TMK1::TMK1-FLAG/tmk1-1* and
561 *UBQ10::TMK1-3xHA* transgenic plants after 1-hour treatment with different concentrations of IAA (5,
562 10 and 100 nM IAA) or DMSO control. Ponceau staining was used as a loading control.

563 (B) Corresponding quantification of TMK1 protein levels normalized to Ponceau, and subsequently to
564 DMSO condition, mean ±SD from 3 independent experiments. One-way ANOVA with Dunnett's
565 multiple comparisons relative to DMSO (****$p<0.0001$).

566 (C) Quantification of TMK1-FLAG phosphorylated upon auxin treatment (10 nM, 1 hour) (see Figure
567 2C). Phosphorylation levels detected with a Phos-tag Biotin Probe were normalized to signal obtained
568 from anti-FLAG detection, and subsequently to the initial value from time point 0. Mean ± SD of 3
569 independent biological replicates. *p*-value for comparison to DMSO was calculated with a two-tailed
570 unpaired t-test (**$p < 0.01$).

571 (D) RT-qPCR time course of relative *TMK1* expression after 10 or 100 nM IAA treatment.
572 Normalization was done to *PP2A* as a reference gene. The expression level at the start of the experiment
573 (T0) was set to a relative value of 1 and statistical comparisons were made to this expression level (*p
574 < 0.05, **$p < 0.01$ and ***$p < 0.001$).

575 (E) Time course of TMK1 and ROP6 protein levels in the membrane fraction of 4-day-old WT or *tmk1-*
576 *1* roots upon auxin treatment (5 nM). Plasma membrane AHA2 H^+ ATPase (immunoblot shown in
577 Figures 2A and 4A) was used as a loading control. We then normalized to initial protein levels at time
578 point 0. Values are mean ± SD from 3 independent experiments. Two-way ANOVA with Dunnett's
579 multiple comparisons (****$p < 0.0001$).

580 **Figure S3.**

581 **Figure S3. TMK1 interacts with PIN2 in an auxin-dependent manner and phosphorylates it.**

582 (A) Co-IP assay showing the interaction of TMK1 with PIN2 upon low auxin treatment (5 nM IAA).
583 Microsomal protein fraction from WT was used as a control for unspecific binding of endogenous
584 PIN2 (shown in Figure 3A, same experiment).

585 (B) FRET-FLIM analysis on transiently expressed *35S::TMK1$^{\Delta KD}$-GFP, 35S::TMK1$^{\Delta KD}$-*
586 *GFP/35S::PIN2-mCherry, 35S::FLS2-GFP* and *35S::FLS2-GFP/35S::PIN2-mCherry* in root
587 protoplasts (the same experiment is shown in Figure 3B). GFP fluorescence lifetime was calculated as
588 described in the Methods section. The heat map depicts fluorescence lifetime values (see Figure 3B for
589 lifetime analysis).

590 (C) *In vitro* kinase assay showing phosphorylation of the 6His-PIN2 HL substrate by TMK1-3xHA in
591 the presence or absence of auxin. Top panel, ^{32}P-autoradiography; middle panel, CBB staining; bottom
592 panel, immunoblot with an anti-HA antibody.

593

594 **Figure S4.**

595 **Figure S4. TMK1 regulates PIN2 stability on the post-transcriptional level.**

596 (A) Time course of PIN2 protein levels in the membrane fraction of 4-day-old WT or *tmk1-1* roots upon
597 auxin treatment (5 nM). Plasma membrane AHA2 H^+-ATPase (immunoblot shown in Figures 2A and
598 4A) was used as a loading control. We then normalized to initial protein levels at time point 0. Values
599 are mean ± SD from 3 independent experiments. Two-way ANOVA with Dunnett's multiple
600 comparisons (****$p < 0.0001$).

601 (B) Left panel: immunoblot of endogenous TMK1 and PIN2 in the microsomal fraction in response to
602 1-hour treatment with 10 nM IAA in WT versus *tmk1-1* roots. Right panel: quantification of protein
603 levels detected with anti-TMK1 and anti-PIN2 antibodies normalized to the loading control, and then to
604 DMSO. Values are mean ± SD from 3 independent experiments. Two-way ANOVA with Dunnett's
605 multiple comparisons (****$p<0.0001$).

606 (C) Comparison of PIN2 expression in WT versus *tmk1-1* upon auxin treatment. Relative expression of
607 PIN2 upon 10 and 100 nM IAA treatment at different time points (0, 5, 60, 120 and 180 minutes).
608 Normalization was done to *PP2A* as a reference gene. The expression level at the start of the experiment
609 was set to the relative value of 1.

610

611

612 **Figure S5.**

613 **Figure S5. *TMK* genes are required for robust gravitropic root bending.**

614 (A) Expression levels of *TMK1, TMK2, TMK3* and *TMK4* determined by RT-qPCR in root samples of
615 4-day-old WT and *tmk1-1, tmk2-1, tmk3-1* and *tmk4-1* seedlings. RNA was extracted in 4 independent
616 biological repeats and the RT-qPCR analysis was performed in 3 technical repetitions. Expression levels
617 were normalized against the expression level of PP2A as a housekeeping gene. Asterisks indicate
618 significantly lower expression levels in the respective mutants, two-tailed unpaired t-tests (****$p <$
619 0.0001 and **$p < 0.01$).

620 (B) Root gravitropism in single mutants of TMK family genes. Root curvature angles were measured
621 every 30 min after reorientation by a 90° rotation. Representative images of 4-day-old WT, *tmk1-1,*
622 *tmk2-1, tmk3-1,* and *tmk4-1* single mutant roots after 3 hours of reorientation.

623 (C) Time course of root tip angle changes and root growth rates, mean ± SEM from 3 independent
624 experiments (n= 30-40). See Table S1 for statistical analysis.

625 (D) Representative images of root bending 3 hours after a 90° rotation of 4-day-old WT and the
626 overexpression line of TMK1 without a cytoplasmic kinase domain (*35S::TMK1*$^{\Delta KD}$*-GFP*).

627 (E) Time course of the gravitropic response including *35S::TMK1*$^{\Delta KD}$*-GFP* lines and root growth rate
628 from the same experiment at the indicated time points, mean ± SD (n = 10; experiment repeated 3 times
629 with representative data depicted).

630 (F) Representative images of primary roots expressing the *UBQ10::TMK1*^{K616R}*-mCherry* and
631 *35S::TMK1*$^{\Delta KD}$*-GFP* constructs.

632

633 **Figure S6.**

634 **Figure S6. Gravistimulation promotes TMK1 stability, phosphorylation state, and downstream**
635 **signalling**

636 (A) Western blotting of total root protein extracts of 4-day-old *TMK1::TMK1-GFP, TMK1::TMK1-*
637 *FLAG/tmk1-1* and *UBQ10::TMK1-3xHA* transgenic plants after 0, 1, 2, 3h of gravistimulation. Ponceau
638 staining was used as a loading control.

639 (B) Corresponding quantification of the relative TMK1 protein levels normalized first to Ponceau, and
640 then to initial protein levels at time point 0, values are mean ± SD from 3 independent experiments.
641 One-way ANOVA with Dunnett's multiple comparisons to timepoint 0 (****$p < 0.0001$).

642 (C) Comparison of TMK1, PIN2, and ROP6 endogenous levels in the membrane fraction during
643 gravistimulation of WT and *tmk1-1* 4-day-old roots. Normalization was to plasma membrane AHA2
644 ATPase (immunoblot analysis shown in Figure 6A), and then to initial protein levels at timepoint 0.
645 Values are mean ± SD from 3 independent experiments. Two-way ANOVA with Dunnett's multiple
646 comparisons to timepoint 0 (****$p < 0.0001$).

647 (D) Quantification of phosphorylated TMK1 levels during gravistimulation (see Figure 6B). TMK1
648 protein levels detected with biotinylated Phos-tag Probe were normalized to the signal obtained from
649 anti-FLAG detection, and then to the initial value from timepoint 0. Values are mean ± SD from 3
650 experiments with 3 independent biological replicates. Two-way ANOVA with Dunnett's multiple
651 comparisons to timepoint 0 (****$p < 0.0001$).

652

653 **SUPPLEMENTARY TABLES**

654

655 **Table S1. Statistical analysis of the gravitropic kinetics presented in Figure S5B and S5C.** Asterisks
656 are from Dunnett's multiple comparison tests versus WT. *p < 0.05, **p < 0.01, ***p < 0.001, ****p <
657 0.0001.

Time (h)	*tmk1-1*	*tmk2-1*	*tmk3-1*	*tmk4-1*
0.5	ns	ns	ns	ns
1	**	ns	ns	ns
1.5	*	ns	ns	ns
2	*	ns	ns	ns
2.5	*	ns	ns	ns
3	*	ns	ns	ns
3.5	**	ns	ns	ns
4	**	ns	ns	**
4.5	***	ns	ns	*
5	****	ns	ns	*
5.5	****	ns	ns	**
6	****	ns	ns	**
6.5	****	ns	ns	*
7	***	ns	*	*

658

659

660

661

662

663

664

665

666

667

668

669 **Table S2. Statistical analysis of the gravitropic kinetics presented in Figure 5A, 5B, S5D and**
670 **S5E.** Asterisks are from Dunnett's multiple comparison tests versus WT. *p < 0.05, **p < 0.01, ***p
671 < 0.001, ****p<0.0001.

672

Time (h)	*tmk1-1*	*TMK1::TMK1-FLAG/ tmk1-1*	*35S::TMK1ΔKD-GFP WT (L9)*	*35S::TMK1ΔKD-GFP WT (L8)*	*UBQ10::TMK1K616R- mCherry WT (L11)*	*UBQ10::TMK1K616R- mCherry WT (L14)*
0.5	****	ns	*	**	*	ns
1	****	ns	**	**	****	**
1.5	***	ns	*	**	****	**
2	***	ns	*	***	****	**
2.5	****	ns	*	***	****	**
3	****	ns	*	***	****	*
3.5	****	ns	*	*	***	*
4	****	ns	ns	*	***	ns
4.5	****	ns	ns	*	**	ns
5	****	ns	ns	ns	*	*
5.5	****	ns	ns	ns	*	*
6	****	ns	ns	ns	*	**
6.5	****	ns	ns	ns	*	ns
7	***	ns	ns	ns	*	ns

673

674

675

676

677

678

679

680

681 **Table S3. List of primer sequences used in this study.**

682

Primer name	Use	Sequence 5'→ 3'
PP2A FW	RT-qPCR	TAACGTGGCCAAAATGATGC
PP2A RE	RT-qPCR	GTTCTCCACAACCGCTTGGT
EF1a FW	RT-qPCR	TGAGCACGCTCTTCTTGCTTTCA
EF1a RE	RT-qPCR	GGTGGTGGCATCCATCTTGTTACA
TMK1 FW	RT-qPCR	TGGCACCCGAATACGCAGTAAC
TMK1 RE	RT-qPCR	GCTTTCTTCTGGTTGCGATTCGTC
TMK2 FW	RT-qPCR	TTTGGTTTAGTCCGGCTTGC
TMK2 RE	RT-qPCR	CGACCCGTTAGTAGCTCCAT
TMK3 FW	RT-qPCR	ACTCGAGTAGCTGGGACTTTCG
TMK3 RE	RT-qPCR	CACTCTTCCCGTCACTGCGTATTC
TMK4 FW	RT-qPCR	CAGAATACGCCGCTACTGGAAG
TMK4 RE	RT-qPCR	TCCATGAGAACCACACCAAATGC
PIN1 FWa	RT-qPCR	TTACTCCACCGCTACGAAC
PIN1 REa	RT-qPCR	ACTAAACTCTTCCCTCTCCAC
PIN2 FWa	RT-qPCR	TCACGACAACCTCGCTACTAAAGC
PIN2 REa	RT-qPCR	TGCCCATGTAAGGTGACTTTCCC
TMK1-FL-B1-F	cloning	GGGGACAAGTTTGTACAAAAAAGCAGGCTCAATGAAGAAAAGAAGAACCTTTC
TMK1-FL-B2-R	cloning	GGGGACCACTTTGTACAAGAAAGCTGGGTCTCGTCCATCTACTGAAGTGAAT
TMK1-ΔKD-B2-R	cloning	GGGGACCACTTTGTACAAGAAAGCTGGGTCGTTGTTAGTCACAGAACGAAG
TMK1KD-K616F	cloning	ATTGCGGTTAGGAGAATGGAGAATGGAGTTATTGCTGG
TMK1KD-K616R	cloning	CCATTCTCCATTCTCCTAACCGCAATCTTCGTTCCATC
pTMK1-B4-F	cloning	GGGGACAACTTTGTATAGAAAAGTTGCATCGTTTGGAACAGATCTTTCAGC
pTMK1-B1-R	cloning	GGGGACTGCTTTTTTGTACAAACTTGCAGCTTGAAGAAACAGAGGATTGAAG

pTMK2-B4-F	cloning	GGGGACAACTTTGTATAGAAAAGTTGCAGTAGAGGAATGTCGTTGATACCAC
pTMK2-B1-R	cloning	GGGGACTGCTTTTTTGTACAAACTTGCTTTCAACTGAGAAACAAACGCAGGG
pTMK3-B4-F	cloning	GGGGACAACTTTGTATAGAAAAGTTGCAGCCAATCAACAACCCTTTAATCG
pTMK3-B1-R	cloning	GGGGACTGCTTTTTTGTACAAACTTGCTTGTTGGAGAAAGAAACAGAGTGGA
pTMK4-B4-F	cloning	GGGGACAACTTTGTATAGAAAAGTTGCAACTCACAACTCCGTCGATCA
pTMK4-B1-R	cloning	GGGGACTGCTTTTTTGTACAAACTTGCATTAGAGAACACGCGCGGC
tmk1-1-F	genotyping	CCAGTTCCTGCGTCTTTGTT
tmk1-1-R	genotyping	TTAACCGCAATCTTCGTTCC
tmk2-1-R	genotyping	TTTCTCATTCCATGTTCCAGC
tmk2-1-F	genotyping	ACAAGGGAGAGTTGCATGATG
tmk3-1-R	genotyping	TATCAACACCAACGGATTTGC
tmk3-1-F	genotyping	TTGCCAGCTGTATTCACACAC
tmk4-1-F	genotyping	GTGGAATATCTCCATAGCTTGGCT
tmk4-1-R	genotyping	CCACAATTAAAACACAGCCTGTAA

683

684

685

686

687

688

689

690

691

692

693

694

695 **METHODS**

696 **Plant materials and growth conditions.**

697 All mutants and transgenic lines are in the *Columbia-0* (*Col-0*) ecotype background with the exception
698 of *abp1-TD1*, which is in *Columbia-4* (*Col-4*). The T-DNA insertion lines *eir1-4* (SALK_091142) [*pin2*
699 mutant used in Figure 1], *tmk1-1* (SALK_016360), *tmk2-1* (SAIL_1242_H07), *tmk3-1* (SALK_129759)
700 and *tmk4-1* (GABI_348E01) were previously reported[35,59], as was *abp1-C1* and *abp1-TD1*[60], and *comp-*
701 *C1* = (*ABP1::GFP-ABP1/abp1-C1*)[61]. The primers for genotyping are described in Supplementary
702 Table 3. *PIN2::PIN2-GFP*, *DR5rev::GFP* and *TMK1::TMK1-FLAG* in *tmk1-1* (*comp-tmk1-1*) were
703 described[59,62,63]. *DEX::TMK1*^{K616R}*-HA* line (unpublished) was kindly provided by William Gray. We
704 generated transgenic lines *PIN2::PIN2-GFP* in *tmk1-1* and *DR5rev::GFP* in *tmk1-1* by crossing the
705 respective markers and the mutant line.

706 To generate *TMK1::GUS, TMK2::GUS, TMK3::GUS, and TMK4::GUS* transgenic lines, genomic
707 fragments covering 2000 bp upstream from the start codon of *TMK1, TMK2, TMK3* and *TMK4* were
708 amplified from *Col-0* genomic DNA as a promotor region. We used these primers for amplification:
709 *pTMK1-B4-F/pTMK1-B1-R, pTMK2-B4-F/pTMK2-B1-R, pTMK3-B4-F/pTMK3-B1-R, pTMK4-B4-*
710 *F/pTMK4-B1-R* (see sequences in Supplemental Table 3). The promoter fragments were inserted into
711 *pDONR P4-P1r* vector by BP recombination reaction, resulting in *pDONR P4-P1R pTMK1, pDONR*
712 *P4-P1R pTMK2, pDONR P4-P1R pTMK3, and pDONR P4-P1R pTMK4* plasmids. Those products were
713 subsequently cloned into pB7m24GW.3 vector together with pEN-L1-GUS-L2 (Invitrogen) by
714 MultiSite Gateway LR recombination reaction. To generate *TMK1::TMK1-GFP, 35S::TMK1*$^{\Delta KD}$*-GFP*
715 expressing lines, the *TMK1* full length/ *TMK1*$^{\Delta KD}$ (amino acid 1-587) genomic DNA without stop codon
716 were amplified from DNA of *Col-0* seedlings by PCR using *TMK1-FL-B1-F* and *TMK1-FL-B2-*
717 *R/TMK1-ΔKD-B2-R* primers (see sequences Supplemental Table 3), respectively. The corresponding
718 *TMK1* DNA sequences were inserted into pDONR221 vector by BP recombination reaction. Next, for
719 *TMK1::TMK1-GFP* construct, *pDONR P4-P1R pTMK1, pDONR221 gTMK1* and *pDONR P2R-P3*
720 *GFP*; for *35S::TMK1*$^{\Delta KD}$*-GFP, pDONR P4-P1R p35S, pDONR221 gTMK1*$^{\Delta KD}$ and *pDONR P2R-P3*
721 *GFP* were cloned into pB7m34GW vector by MultiSite Gateway LR recombination reaction. To
722 generate *UBQ10::TMK1*^{K616R}*-2xmCherry*, *TMK1*^{K616R}*noSTOP/pDONR221* was obtained by site directed
723 mutagenesis, amplifying *pDONR221 TMK1* with the *TMK1KD-K616F/TMK1KD-K616R* primer pair.
724 *pDONR221 TMK1*^{K616R} was then recombined by LR reaction with *pDONR P4-P1R pUBQ10*[64], *pDONR*
725 *P2R-P3 2xmCHERRY-4xMyc*[65] and pH7m34GW[66] to introduce *UBQ10::TMK1*^{K616R}*-2xmCherry* in
726 pH7m34GW. All constructs were transformed into the *Agrobacterium tumefaciens* strain pGV3101 by
727 electroporation and further into *Col-0* plants by floral dip method. After being selected for single-copy
728 insertions, two individual homozygous T3 transgenic lines were used for further studies.

729 *Arabidopsis thaliana* seeds were surface-sterilized with 70% (v/v) ethanol for 20 min, followed by
730 commercial bleach (2.5% [v/v] sodium hypochlorite) containing 0.05% (v/v) Triton X-100 for 10 min,
731 and finally washed four times with sterile distilled water. The stratification of the seeds was conducted
732 in the dark at 4°C for 3 days. *Arabidopsis thaliana* seedlings were grown at 22°C on ½ MS plates with
733 1% agar and 1% sucrose, or in soil with 16h light/8h dark cycles, photoperiod at 80 to 100 mE m^{-2} sec^{-}
734 ^{1}.
735
736 **Measurement of basipetal auxin transport in roots**
737 Root basipetal auxin transport measurement was executed as previously described[67]. Briefly, 5-day-old
738 *Arabidopsis* seedlings were neatly placed on ½ MS plates and vertically grown for around 12 hours. 100
739 nM ^{3}H -IAA droplets were prepared by adding 2 µl of 25 Ci $mmol^{-1}$ ^{3}H -IAA to 1 ml ½ MS with 1.25
740 % agar and quickly added dropwise onto a humid petri dish lid. Then the auxin-containing droplets were
741 carefully placed on root tips with about 0.5 mm overlap. Transport was allowed for 5 hours in darkness
742 at room temperature. 2 mm of root tissue proximal to the site of auxin application was discarded, and
743 an 8-mm root segment was cut from the rest of the root tip and harvested to 3 ml of scintillation fluid.
744 Radioactivity was counted with a scintillation counter (HIDEX 300 SL) for 100 seconds. 10 seedlings
745 were used for each treatment with 3 repetitions.
746
747 **Measurement of basipetal auxin transport in shoots**
748 Shoot basipetal auxin transport was carried out as previously described[68]. Briefly, surface-sterilized
749 A*rabidopsis thaliana* seeds were stratified in the dark at 4°C for 72 h, placed in the light for 6 hours to
750 induce germination and transferred to the darkness at 22°C for 5 days. Then, 5-day-old etiolated
751 hypocotyls were decapitated to exclude the effect of auxin biosynthesis in cotyledons and ^{3}H -IAA
752 droplets (60 nM: 12 µL ^{3}H-IAA in 10 mL of ½ MS medium with 1.25% agar) were carefully applied to
753 the apical part of the hypocotyls. After 6 hours incubation, treated hypocotyls were collected,
754 homogenized in liquid nitrogen and incubated overnight in Opti-Fluor scintillation cocktail (Perkin
755 Elmer). Finally, the radioactivity was measured with a scintillation counter (Hidex 300SL) for
756 300 seconds. 10 seedlings were used for each treatment with 3 repetitions. An additional background
757 control for any diffusion though the agar was performed by inserting the droplet above the decapitated
758 hypocotyl and treatment with 10 µM NPA as a negative control.
759
760 **Mutant evaluation and expression analysis by RT-qPCR.**
761 For RT-qPCR analyses, total RNA was prepared from max. 100mg of roots of 4-day-old seedlings
762 according to the RNeasy Plant Mini Kit (Qiagen). cDNA was synthesized from 1µg of total mRNA
763 using the QuantiNova Reverse Transcription Kit (Qiagen). For all mutant expression analyses, four

764 biological replicates were considered, and the samples were pipetted in three technical replicates into a
765 384 well plate using an automated JANUS Workstation (PerkinElmer). According to the manufacturer's
766 instructions, 5 µL reaction volume contained 2.5 µL Luna® Universal qPCR mastermix (NEB). RT-
767 qPCR analyses were performed using the Real-time PCR Roche Lightcycler 480 and the expression of
768 PP2AA3 (At1G13320) was used as in[69]. For each of the evaluated genes, three different primer pairs
769 were evaluated, and representative graphs are enclosed in the manuscript. The primers used for the
770 presented analyses are listed in Supplemental Table 3.
771
772 **Förster Resonance Energy Transfer with Fluorescence Lifetime Imaging Microscopy (FRET-**
773 **FLIM).**
774 FRET-FLIM experiments were performed in protoplast systems isolated from *Arabidopsis* root cell
775 suspension as described previously[70]. 10 µg of plasmid DNA (*TMK1-GFP, TMK1*$^{\Delta KD}$*-GFP, PIN2-*
776 *mCherry, FLS2-GFP*) were used for protoplast transfection and then incubated in a sterile 24-well
777 microtiter plate overnight in the dark at room temperature. FRET-FLIM experiments were performed
778 using a TriM Scope II inverted 2-photon microscope equipped with a FLIM X16 TCSPC Detector for
779 time correlated single photon counting (LaVision BioTec). Fluorescence lifetime image stacks (150
780 slices, with 0,082 ns time interval) were acquired. Image analyses were done in Fiji by performing a
781 threshold mask from the sum projection of each stack and by averaging all the pixels at each time point
782 of the stack. In order to yield the exponential decay with offset, the intensity at time point 0 was
783 normalized.
784
785 **Histochemical GUS staining.**
786 4-day-old seedlings of *TMK1::GUS, TMK3::GUS and TMK4::GUS* were stained in 0.1 M sodium
787 phosphate buffer (pH 7.0) containing 0.1% X-GlcA sodium salt, 1 mM $K_3[Fe(CN)_6]$, 1 mM $K_4[Fe(CN)_6]$
788 and 0.05% Triton X-100 for 20 min (TMK1::GUS), 2 h (TMK4::GUS) or 6 h (TMK3::GUS) at 37°C.
789 Further, samples were incubated overnight in 80% (v/v) ethanol at room temperature. Tissue clearing
790 was conducted as previously described[71]. DIC microscopy for analysis of GUS staining assay was
791 performed using an Olympus BX53 microscope equipped with 10x and 20x air objectives and a DP26
792 CCD camera.
793
794 **Root Gravitropic Assay.**
795 For measurements of root gravitropic curvature kinetics and growth rate, 4-day-old seedlings were
796 rotated 90° and roots were imaged every 30 min on a vertically placed flatbed scanner (Epson Perfection
797 V370 Photo). Image time series were stabilized using the StackReg Fiji plugin. Root curvature angle
798 (including root tip angle and rate of change) along with growth rate were analyzed using the Manual
799 Tracking Fiji plugin and Microsoft Excel.
800

801 **Imaging with confocal laser scanning microscopy (CLSM).**

802 Confocal laser scanning microscopy for analysis of fluorescent intensity was performed on Zeiss
803 LSM800 microscope, positioned vertically[72], assisted with Zeiss Zen 2011 software. Pictures were taken
804 by 20x objectives. Fluorescence signals for GFP (excitation 488 nm, emission 507 nm) and mCherry
805 (excitation 561 nm; emission 580-650 nm)-tagged proteins were detected.

806 For the analysis of *PIN2::PIN2-GFP, DR5rev::GFP* and *TMK1::TMK1-GFP* asymmetric distribution
807 during gravistimulation, 4-day-old seedlings were placed in a 1-well chambered coverglass (VWR,
808 Kammerdeckgla¨ ser, Lab-Tek, Nunc - eine kammer, catalog number 734-2056) with a block of solid
809 0.5 MS medium (as described in [72]). In order to adjust seedlings to the new gravity vector, the chamber
810 with samples was transferred to the darkness 1 h prior CLSM analysis, at the vertical position. Ten Z-
811 sections spaced 4.5 mm for *PIN2* line and 1 mm for *DR5rev* and *TMK1* promoter analysis were collected
812 in the median root section before and after 90° rotation at the indicated time points. Pictures were
813 subsequently combined into the *sum* slices intensity projection. Marking epidermal and cortical regions
814 together, the mean grey value of the signal intensity was collected and used for quantification (as
815 described previously in [36]).

816

817 **Protein extraction and western blot analysis.**

818 Roots from 4-day-old seedlings expressing *TMK1::TMK1-GFP*, *TMK1::TMK1-FLAG* or
819 *UBQ10::TMK1-3xHA* after gravistimulation or auxin treatments were frozen and grounded to powder
820 in a liquid nitrogen. To analyze the *TMK1*-tagged expression level, proteins were isolated in a mixture
821 of: 50 mM Tris–HCl pH 7.5, 150 mM NaCl, 5 mM dithiothiothreitol (DTT), 1 mM Na_2MoO_4•$2H_2O$, 1
822 mM NaF, 1% TritonX100, Complete EDTA-free Protease Inhibitor cocktail (Roche), PhosSTOP
823 phosphatase inhibitor cocktail (Roche) and clarified by 15 min centrifugation step at 12000 g, 4°C. The
824 analysis was carried out by SDS-PAGE and western blots using Anti-GFP HRP-conjugated (MACS
825 Miltenyi Biotec), anti-FLAG®M2-Peroxidase (HRP) (Sigma), Anti-HA HRP-conjugated, High Affinity
826 (3F10) (Roche) and SuperSignal West Femto Maximum Sensitivity Substrate Detection System
827 (Thermo Scientific). Equal loading was ensured by Bradford protein quantification before loading, and
828 by Ponceau staining of the membrane after protein transfer. Image capture was done using the image
829 analyzer Amersham 600RGB 604 (GE Healthcare), and quantification of the protein signal was done
830 using Fiji software.

831

832 **Protein microsomal fraction extraction.**

833 4-day-old seedling roots were harvested, grounded to powder in a liquid nitrogen, and vortexed
834 vigorously in extraction buffer 1 (50 mM Tris–HCl pH 7.5, 150 mM NaCl, Complete EDTA-free
835 Protease Inhibitor cocktail (Roche), PhosSTOP phosphatase inhibitor cocktail (Roche)) in 1/10 (w/v)
836 ratio. The resulting homogenate was centrifuged at 20000 g for 30 min at 4°C. The pellet was

837 resuspended in extraction buffer 2 (50 mM Tris–HCl pH 7.5, 150 mM NaCl, 0.5% Nonidet P-40, 1%
838 TritonX100, Complete EDTA-free Protease Inhibitor cocktail (Roche), PhosSTOP phosphatase
839 inhibitor cocktail (Roche)), and centrifuged at 12000 g for 20 min at 4°C. The supernatant was used for
840 total protein concentration quantification by Bradford assay. Samples were separated by SDS-PAGE (4-
841 15% Mini-PROTEAN®TGX™ Precast Protein Gels (Bio-RAD)), transferred to a PVDF
842 (polyvinylidene difluoride) membrane and analyzed by immunoblot using the following primary
843 antibodies: affinity-purified TMK1 (1:1000, [59]), AHA2 (1:1000, [73]) and PIN2 (1:1000, [35]) antibodies and
844 anti-ROP6 (C) (1:1000, Abiocode), using anti-Rabbit HRP-conjugated (1:5000, GE Healthcare) as a
845 secondary antibody. Detection was performed using the SuperSignal West Femto Maximum Sensitivity
846 Substrate detection kit (ThermoFisher Scientific). Image capture was done using the image analyzer
847 Amersham 600RGB (GE Healthcare), and quantification of the protein signal was done using Fiji
848 software.
849
850 **Western blot analysis of phosphorylated proteins.**
851 To analyze the phosphorylation status of TMK1 *in planta*, after corresponding treatment, 4-day-old
852 *tmk1-1* roots expressing *TMK1::TMK1-FLAG* were grounded to powder in liquid nitrogen and
853 homogenized in ice-cold sucrose buffer (20 mM Tris–HCl pH 8, 0.33 M sucrose, Complete EDTA-free
854 Protease Inhibitor cocktail (Roche), PhosSTOP phosphatase inhibitor cocktail (Roche)), followed by a
855 centrifugation step at 5000 g for 10 min at 4°C. To obtain the membrane protein fraction, the supernatant
856 was centrifuged at 20000 g for 30 min at 4°C and the resulting pellet was solubilized with lysis buffer
857 (20 mM Tris–HCl pH 8, 150 mM NaCl, 1% TritonX100, Complete EDTA-free Protease Inhibitor
858 cocktail (Roche), PhosSTOP phosphatase inhibitor cocktail (Roche)) and centrifuged at 20000 g for 10
859 min at 4°C. The corresponding supernatant was used for immunoprecipitation assay with anti-FLAG
860 micro beads according to the manufacturer´s instructions (µMACS Epitope Tag Protein Isolation Kit
861 (MACS Miltenyi Biotec)). Samples were separated by SDS-PAGE (4-15% Mini-PROTEAN®TGX™
862 Precast Protein Gels (Bio-RAD)) and transferred to a PVDF membrane followed by probe with Phos-
863 tag BTL-111 according to the manufacturer's instructions (www.wako-chem.co.jp) to detect protein
864 phosphorylated levels and anti-FLAG®M2-Peroxidase (HRP) (Sigma) antibody to detect the total
865 amount of immunoprecipitated TMK1-FLAG.
866
867 **Co-Immunoprecipitation assays.**
868 4-day-old *tmk1-1* seedlings expressing *TMK1::TMK1-FLAG* were treated with 5, 20 nM IAA or DMSO
869 control for 30 minutes. Roots were harvested, grounded to powder in liquid nitrogen, and subjected to
870 protein microsomal fraction extraction. Solubilized proteins from microsomal fraction were
871 immunoprecipitated using super-paramagnetic micro MACS beads coupled to monoclonal anti-FLAG
872 antibody according to the manufacturer´s instructions (Miltenyi Biotec). WT *Col-0* extract was used as
873 a control of the unspecific binding of endogen PIN2. Proteins immunoprecipitated with anti-FLAG

874 antibody were separated by SDS-PAGE (4-15% Mini-PROTEAN®TGX™ Precast Protein Gels (Bio-
875 RAD)), transferred to a PVDF membrane and analyzed by immunoblot with anti-FLAG®M2-Peroxidase
876 (HRP) (Sigma) antibody to detect TMK1-FLAG and with anti-PIN2 antibody to detect co-
877 immunoprecipitated endogenous PIN2.
878
879 **Active ROP assay of non-overexpressing plants**

880 5-day-old seedling roots were excised and incubated in ½ MS liquid medium. The roots were treated
881 with 100 nM IAA for 10 minutes and frozen in liquid nitrogen. Total protein was extracted from the
882 treated root tissues using Extraction buffer (25mM HEPES pH 7.4, 100mM KCl, 10mM MgCl2, 1 mM
883 PMSF, 5 mM Na3VO4, 5 mM NaF, 1 mM TCEP, cOmplete Protease Inhibitor Cocktail, Roche) in 2
884 steps. For every 100 mg of grounded tissue, 400 µl of extraction buffer were added, then incubated with
885 another 400 µl of extraction buffer containing 5% Triton X-100 for one hour. Active ROP proteins were
886 pulled down using His-MBP-CRIB (originally from RIC1 effector, obtained from expressing BL21
887 *E.coli* total cell extract) conjugated to HisPur™ Ni-NTA Magnetic Beads (Thermo Fisher) by incubation
888 of 200 µl total protein extract with 25 µl (initial volume) of beads for 2 hours at 4°C. The beads were
889 washed by Washing buffer (25 mM HEPES pH 7.4, 300 mM KCl, 10 mM $MgCl_2$, 12.5 mM imidazole)
890 for 3 times and boiled at 95°C with 30 µl SDS loading dye (BioRad). After removing the beads, the
891 protein samples were separated by 12% SDS-PAGE and analyzed by immunoblot with anti-ROP2
892 specific antibody (1:10,000, Abiocode). Input samples were isolated from total protein extracts, before
893 addition of Triton X-100 to get an estimate of the present total ROP content.

894

895 **Quantitative immunoblot analysis.**
896 To determine the relative amount of protein in time course experiments, grey values were calculated by
897 ImageJ Gel Analysis tool, where for each band of protein of interest (PI) and normalizing control (NC),
898 membrane background was removed individually. To get relative NC value, all the NC values were
899 divided by the highest one. Subsequently, all the PI values were divided by their respective relative NC
900 values. Final obtained values of PI were normalized dividing by the time point 0 or DMSO control
901 treatment value. Values from three independent experiments were used to determine average and ±SD.
902 For example, for quantitative immunoblot analysis of phosphorylated proteins, it was first determined
903 grey values of TMK1 obtained with Phos-tag BTL-111 probe and anti-Flag antibody at different time
904 points/treatments, tacking into account each membrane background. TMK1-Flag values were used as a
905 protein amount normalizing control (NC). To get NC values of each experiment point, TMK1-Flag
906 values were divided by the highest one. Subsequently, TMK1 Phos-tag values were divided by their
907 respective relative NC values. To compare differences between time points/ treatments, as a final step,

908 the normalized at protein level TMK1 Phos-tag values were divided by the corresponding time point 0
909 or DMSO control treatment values.
910
911 **Recombinant protein expression and purification from *E. coli.***
912 The 6xHis-PIN2 HL recombinant protein was expressed using the 6xHis-PIN2 HL vector [74] in *E. coli*
913 BL21 (DE3) strain upon induction by 0.5 mM IPTG (Isopropyl β-D-1-Thiogalactopyranoside) at 16°C
914 for 12 h. Cells were harvested by centrifugation at 4000 g for 15 min and washed with water. They were
915 then lysed by sonication in lysis buffer (50 mM Tris-HCl pH7.5; 150 mM NaCl; 1 mM EDTA; 1 mM
916 DTT and 1% TritonX100). The lysed solution was centrifuged at 12000 g for 15 min. The supernatant
917 was then purified using Ni-NTA His affinity agarose (Thermo Scientific) according to the
918 manufacturer's instructions. 6xHis- PIN2 HL protein was eluted from the beads in elution buffer (50
919 mM Tris-HCl pH7.4; 150 mM NaCl and 250 mM imidazole). Eluted protein samples were checked by
920 SDS-PAGE and Coomassie brilliant blue staining (Bio-Safe™ Coomassie Stain, Bio-Rad). The protein
921 concentration was determined with the Bradford method (Quick Start™ Bradford Reagent, Bio-Rad).
922
923 **TMK1-HA immunoprecipitation.**
924 To immunoprecipitate HA-tagged TMK1 protein, roots of 7-day-old *pUBQ10::TMK1-3xHA* and
925 *DEX::TMK1^{K616R}-HA* (previously induced for 48 h with 30 μM dexamethasone) seedlings were frozen
926 and grounded in a liquid nitrogen, and, subsequently, homogenized in protein extraction buffer (PEB:
927 50 mM Tris-HCl pH7.5, 200 mM NaCl, 1% TritonX100, 10 mM $MgCl_2$, 1 mM $MnCl_2$, Complete
928 (Roche) protease cocktail and PhosSTOP phosphatase inhibitor cocktail (Roche)), followed by the 20
929 min centrifugation step at 14000 g, 4°C. In a fresh Eppendorf tube, 50 μL anti-HA agarose beads were
930 added (Anti-HA Affinity Matrix, SIGMA; pre-washed with 200 μL PEB) to the supernatant. After 4 h
931 of rotating at 4°C, the samples were spun down again at 2000 g, 4°C, and the supernatant was discarded.
932 The Agarose beads were washed twice with 200 μL PEB, and finally re-suspended into 50 μL PEB to
933 allow further biochemical reactions.
934
935 ***In vitro* kinase assay.**
936 The *in vitro* kinase assay with [γ-^{32}P]-ATP was conducted as reported[74] with minor modifications.
937 Immunoprecipated TMK1-HA and TMK1^{K616R}-HA (5 μL) from 7-day-old *Arabidopsis* seedlings,
938 together with the recombinant 6xHis-PIN2 HL (10 μL) from *E.coli*, were added to the kinase reaction
939 buffer (50 mM Tris-HCl pH 7.5, 10 mM $MgCl_2$, 5 mM NaCl, 2.5 mM cold ATP (adenosine 5'-
940 triphosphate), and 1 mM DTT) in the presence of 5 μCi [γ-^{32}P]-ATP (NEG502A001MC; Perkin-Elmer).
941 Reactions were incubated at 25°C for 90 min and afterwards terminated by adding 10 μL 5×SDS loading
942 buffer. 20 μL reaction samples were then separated with 10% SDS-PAGE gel, developed with a
943 phosphor-plate overnight. Eventually, the phosphor-plate was imaged with a Fujifilm FLA 3000 plus
944 DAGE system.

945

946 **Statistical analysis.**

947 Data visualization was conducted using the GraphPad Prism 8 Software or in R version 4.0.4. For
948 statistical comparisons we used standard linear models (t-test, one- or two-way ANOVA with Dunnett's
949 multiple comparisons) after first checking their assumptions. Some charts in Figure 1 represent pooled
950 data from multiple experiments. In such cases, we fitted mixed linear models with *restricted maximum*
951 *likelihood* using the *lme()* function implemeted as part of the *nlme* R package. We tested the influence
952 of genotype/treatment as a fixed effect (type II analysis of deviance) and included experimental
953 repetition as a random effect. The random effect was tested by comparing a model where it was included
954 to a model with just the fixed effect using the *gls()* function. The result was reported as the amount by
955 which the Akaike Information Criterion (AIC) of the model increased when excluding the random effect,
956 along with the associated p-value.

957

958 **Accession Numbers**

959 Sequence data from this article can be found in the *Arabidopsis* Genome Initiative databases under the
960 following accession numbers: At4g02980 for *ABP1*, At1g66150 for *TMK1*, At1g24650 for *TMK2*,
961 At2g01820 for *TMK3*, At3g23750 for *TMK4*, At5g57090 for *PIN2*, At1g20090 for *ROP2*, At4g35020
962 for *ROP6*, At4g30190 for *AHA2*, At5g46330 for *FLS2.*

963

964

965

966

967

968

969

970

971

972

973

974

975

REFERENCES

1. Darwin, C., and Darwin, F. (1897). The Power of Movement in Plants. Appleton.

2. Friml, J. (2021). Fourteen Stations of Auxin. Cold Spring Harb. Perspect. Biol. *14*, a039859. 10.1101/cshperspect.a039859.

3. Berleth, T., and Sachs, T. (2001). Plant morphogenesis: Long-distance coordination and local patterning. Curr. Opin. Plant Biol. *4*, 57–62. 10.1016/S1369-5266(00)00136-9.

4. Hajný, J., Tan, S., and Friml, J. (2022). Auxin canalization: From speculative models toward molecular players. Curr. Opin. Plant Biol. *65*, 102174. 10.1016/J.PBI.2022.102174.

5. Zhang, J., Mazur, E., Balla, J., Gallei, M., Kalousek, P., Medveďová, Z., Li, Y., Wang, Y., Prát, T., Vasileva, M., et al. (2020). Strigolactones inhibit auxin feedback on PIN-dependent auxin transport canalization. Nat. Commun. *11*, 1–10. 10.1038/s41467-020-17252-y.

6. Adamowski, M., and Friml, J. (2015). PIN-dependent auxin transport: Action, regulation, and evolution. Plant Cell *27*, 20–32. 10.1105/tpc.114.134874.

7. Luschnig, C., and Vert, G. (2014). The dynamics of plant plasma membrane proteins: PINs and beyond. Dev. *141*, 2924–2938. 10.1242/dev.103424.

8. Park, J., Lee, Y., Martinoia, E., and Geisler, M. (2017). Plant hormone transporters: what we know and what we would like to know. BMC Biol. *15*, 1–15. 10.1186/S12915-017-0443-X.

9. Péret, B., Swarup, K., Ferguson, A., Seth, M., Yang, Y., Dhondt, S., James, N., Casimiro, I., Perry, P., Syed, A., et al. (2012). AUX/LAX Genes Encode a Family of Auxin Influx Transporters That Perform Distinct Functions during Arabidopsis Development. Plant Cell *24*, 2874–2885. 10.1105/tpc.112.097766.

10. Zhang, J., Nodzyński, T., Pěnčík, A., Rolčík, J., and Friml, J. (2010). PIN phosphorylation is sufficient to mediate PIN polarity and direct auxin transport. Proc. Natl. Acad. Sci. U. S. A. *107*, 918–922. 10.1073/pnas.0909460107.

11. Wisniewska, J., Xu, J., Seifartová, D., Brewer, P.B., Růžička, K., Blilou, L., Rouquié, D., Benková, E., Scheres, B., and Friml, J. (2006). Polar PIN localization directs auxin flow in plants. Science *312*, 883. 10.1126/science.1121356.

12. Prigge, M.J., Platre, M., Kadakia, N., Zhang, Y., Greenham, K., Szutu, W., Pandey, B.K., Bhosale, R.A., Bennett, M.J., Busch, W., et al. (2020). Genetic analysis of the Arabidopsis

1007 TIR1/ AFB auxin receptors reveals both overlapping and specialized functions. Elife *9*,
1008 e54740.

1009 13. Qi, L., Kwiatkowski, M., Chen, H., Hoermayer, L., Sinclair, S., Zou, M., Del Genio, C.I.,
1010 Kubeš, M.F., Napier, R., Jaworski, K., et al. (2022). Adenylate cyclase activity of TIR1/AFB
1011 auxin receptors in plants. Nature *611*, 133–138. https://doi.org/10.1038/s41586-022-05369-7.

1012 14. Li, L., Verstraeten, I., Roosjen, M., Takahashi, K., Rodriguez, L., Merrin, J., Chen, J., Shabala,
1013 L., Smet, W., Ren, H., et al. (2021). Cell surface and intracellular auxin signalling for H+
1014 fluxes in root growth. Nature *599*, 273–277. 10.1038/s41586-021-04037-6.

1015 15. Friml, J., Gallei, M., Gelová, Z., Johnson, A., Mazur, E., Monzer, A., Rodriquez, L., Roosjen,
1016 M., Verstraeten, I., Živanovič, B.D., et al. (2022). ABP1–TMK auxin perception for global
1017 phosphorylation and auxin canalization. Nature *609*, 575–581. 10.1038/s41586-022-05187-x.

1018 16. Xu, T., Dai, N., Chen, J., Nagawa, S., Cao, M., Li, H., Zhou, Z., Chen, X., De Rycke, R.,
1019 Rakusová, H., et al. (2014). Cell surface ABP1-TMK auxin-sensing complex activates ROP
1020 GTPase signaling. Science *343*, 1025–1028. 10.1126/science.1245125.

1021 17. Mazur, E., Kulik, I., Hajný, J., and Friml, J. (2020). Auxin canalization and vascular tissue
1022 formation by TIR1/AFB-mediated auxin signaling in Arabidopsis. New Phytol. *226*, 1375–
1023 1383. 10.1111/NPH.16446.

1024 18. Wabnik, K., Kleine-Vehn, J., Balla, J., Sauer, M., Naramoto, S., Reinö Hl, V., Merks, R.M.,
1025 Govaerts, W., and Friml, J. (2010). Emergence of tissue polarization from synergy of
1026 intracellular and extracellular auxin signaling. Mol. Syst. Biol. *6*, 447. 10.1038/msb.2010.103.

1027 19. Narasimhan, M., Gallei, M., Tan, S., Johnson, A., Verstraeten, I., Li, L., Rodriguez, L., Han,
1028 H., Himschoot, E., Wang, R., et al. (2021). Systematic analysis of specific and nonspecific
1029 auxin effects on endocytosis and trafficking. Plant Physiol. *186*, 1122–1142.
1030 10.1093/PLPHYS/KIAB134.

1031 20. Narasimhan, M., Johnson, A., Prizak, R., Kaufmann, W.A., Tan, S., Casillas-Pérez, B., and
1032 Friml, J. (2020). Evolutionarily unique mechanistic framework of clathrin-mediated
1033 endocytosis in plants. Elife *9*, 1–30. 10.7554/eLife.52067.

1034 21. Naramoto, S., Kleine-Vehn, J., Robert, S., Fujimoto, M., Dainobu, T., Paciorek, T., Ueda, T.,
1035 Nakano, A., Van Montagu, M.C.E., Fukuda, H., et al. (2010). ADP-ribosylation factor
1036 machinery mediates endocytosis in plant cells. Proc. Natl. Acad. Sci. *107*, 21890–21895.
1037 10.1073/pnas.1016260107.

1038 22. Naramoto, S., Otegui, M.S., Kutsuna, N., de Rycke, R., Dainobu, T., Karampelias, M.,
1039 Fujimoto, M., Feraru, E., Miki, D., Fukuda, H., et al. (2014). Insights into the Localization and

1040 Function of the Membrane Trafficking Regulator GNOM ARF-GEF at the Golgi Apparatus in
1041 Arabidopsis. Plant Cell *26*, 3062–3076. 10.1105/TPC.114.125880.

1042 23. Glanc, M., Van Gelderen, K., Hoermayer, L., Tan, S., Naramoto, S., Zhang, X., Domjan, D.,
1043 Včelařová, L., Hauschild, R., Johnson, A., et al. (2021). AGC kinases and MAB4/MEL
1044 proteins maintain PIN polarity by limiting lateral diffusion in plant cells. Curr. Biol. *31*, 1918–
1045 1930. 10.1016/J.CUB.2021.02.028.

1046 24. Tan, S., Zhang, X., Kong, W., Yang, X.L., Molnár, G., Vondráková, Z., Filepová, R., Petrášek,
1047 J., Friml, J., and Xue, H.W. (2020). The lipid code-dependent phosphoswitch PDK1–D6PK
1048 activates PIN-mediated auxin efflux in Arabidopsis. Nat. Plants *6*, 556–569. 10.1038/s41477-
1049 020-0648-9.

1050 25. Xiao, Y., and Offringa, R. PDK1 regulates auxin transport and Arabidopsis vascular
1051 development through AGC1 kinase PAX. *6*, 544–555. 10.1038/s41477-020-0650-2.

1052 26. Zourelidou, M., Absmanner, B., Weller, B., Barbosa, I.C.R., Willige, B.C., Fastner, A., Streit,
1053 V., Port, S.A., Colcombet, J., van Bentem, S. de la F., et al. (2014). Auxin efflux by PIN-
1054 FORMED proteins is activated by two different protein kinases, D6 PROTEIN KINASE and
1055 PINOID. Elife *2014*. 10.7554/ELIFE.02860.

1056 27. Zhang, Y., Xiao, G., Wang, X., Zhang, X., and Friml, J. (2019). Evolution of fast root
1057 gravitropism in seed plants. Nat. Commun. *10*, 1–10. 10.1038/s41467-019-11471-8.

1058 28. Sato, E.M., Hijazi, H., Bennett, M.J., Vissenberg, K., and Swarup, R. (2015). New insights into
1059 root gravitropic signalling. J. Exp. Bot. *66*, 2155–2165. 10.1093/JXB/ERU515.

1060 29. Morita, M.T. (2010). Directional Gravity Sensing in Gravitropism. Annu. Rev. Plant Biol. *61*,
1061 705–720. 10.1146/annurev.arplant.043008.092042.

1062 30. Friml, J., Wisniewska, J., Benkova, E., Mendgen, K., and Palme, K. (2002). Lateral relocation
1063 of auxin efflux regulator PIN3 mediates tropism in Arabidopsis. Nature *415*, 806–809.
1064 10.1038/415806a.

1065 31. Kleine-Vehn, J., Ding, Z., Jones, A.R., Tasaka, M., Morita, M.T., and Friml, J. (2010).
1066 Gravity-induced PIN transcytosis for polarization of auxin fluxes in gravity-sensing root cells.
1067 Proc. Natl. Acad. Sci. U. S. A. *107*, 22344–22349. 10.1073/pnas.1013145107.

1068 32. Luschnig, C., Gaxiola, R.A., Grisafi, P., and Fink, G.R. (1998). EIR1, a root-specific protein
1069 involved in auxin transport, is required for gravitropism in Arabidopsis thaliana. Genes Dev.
1070 *12*, 2175–2187. 10.1101/gad.12.14.2175.

1071 33. Swarup, R., Friml, J., Marchant, A., Ljung, K., Sandberg, G., Palme, K., and Bennett, M.

1072 (2001). Localization of the auxin permease AUX1 suggests two functionally distinct hormone
1073 transport pathways operate in the Arabidopsis root apex. Genes Dev. *15*, 2648–2653.
1074 10.1101/gad.210501.

1075 34. Fendrych, M., Akhmanova, M., Merrin, J., Glanc, M., Hagihara, S., Takahashi, K., Uchida, N.,
1076 Torii, K.U., and Friml, J. (2018). Rapid and reversible root growth inhibition by TIR1 auxin
1077 signalling. Nat. Plants *4*, 453–459. 10.1038/s41477-018-0190-1.

1078 35. Abas, L., Benjamins, R., Malenica, N., Paciorek, T.T., Wiřniewska, J., Moulinier-Anzola, J.C.,
1079 Sieberer, T., Friml, J., and Luschnig, C. (2006). Intracellular trafficking and proteolysis of the
1080 Arabidopsis auxin-efflux facilitator PIN2 are involved in root gravitropism. Nat. Cell Biol. *8*,
1081 249–256. 10.1038/ncb1369.

1082 36. Baster, P., Robert, S., Kleine-Vehn, J., Vanneste, S., Kania, U., Grunewald, W., De Rybel, B.,
1083 Beeckman, T., and Friml, J. (2013). SCFTIR1/AFB-auxin signalling regulates PIN vacuolar
1084 trafficking and auxin fluxes during root gravitropism. EMBO J. *32*, 260–274.
1085 10.1038/emboj.2012.310.

1086 37. Retzer, K., Akhmanova, M., Konstantinova, N., Malínská, K., Leitner, J., Petrášek, J., and
1087 Luschnig, C. (2019). Brassinosteroid signaling delimits root gravitropism via sorting of the
1088 Arabidopsis PIN2 auxin transporter. Nat. Commun. *10*, 1–15. 10.1038/s41467-019-13543-1.

1089 38. Hajný, J., Prát, T., Rydza, N., Rodriguez, L., Tan, S., Verstraeten, I., Domjan, D., Mazur, E.,
1090 Smakowska-Luzan, E., Smet, W., et al. (2020). Receptor kinase module targets PIN-dependent
1091 auxin transport during canalization. Science *370*, 550–557. 10.1126/science.aba3178.

1092 39. Roosjen, M., Kuhn, A., Mutte, S.K., Boeren, S., Krupar, P., Koehorst, J., Fendrych, M., Friml,
1093 J., and Weijers, D. (2022). An ultra-fast, proteome-wide response to the plant hormone auxin.
1094 bioRxiv, 2022.11.25.517949. https://doi.org/10.1101/2022.11.25.517949.

1095 40. Kuhn, A., Roosjen, M., Sumanth, M., Dubey, S.M., Carasco, P.C., Monzer, A., Kohchi, T.,
1096 Nishihama, R., Fendrych, M., Friml, J., et al. (2022). A RAF-like kinase mediates a deeply
1097 conserved, ultra-rapid auxin response. bioRxiv, 2022.11.25.517951.
1098 https://doi.org/10.1101/2022.11.25.517951.

1099 41. Tan, S., Luschnig, C., and Friml, J. (2021). Pho-view of Auxin: Reversible Protein
1100 Phosphorylation in Auxin Biosynthesis, Transport and Signaling. Mol. Plant *14*, 151–165.
1101 10.1016/J.MOLP.2020.11.004.

1102 42. Jia, W., Li, B., Li, S., Liang, Y., Wu, X., Ma, M., Wang, J., Gao, J., Cai, Y., Zhang, Y., et al.
1103 (2016). Mitogen-Activated Protein Kinase Cascade MKK7-MPK6 Plays Important Roles in
1104 Plant Development and Regulates Shoot Branching by Phosphorylating PIN1 in Arabidopsis.

1105 PLOS Biol. *14*, e1002550. 10.1371/journal.pbio.1002550.

1106 43. Abas, L., Kolb, M., Stadlmann, J., Janacek, D.P., Lukic, K., Schwechheimer, C., Sazanov,
1107 L.A., Mach, L., Friml, J., and Hammes, U.Z. (2020). Naphthylphthalamic acid associates with
1108 and inhibits PIN auxin transporters. Proc. Natl. Acad. Sci. U. S. A. *118*, 1–8.
1109 10.1073/pnas.2020857118.

1110 44. Pan, X., Fang, L., Liu, J., Senay-Aras, B., Lin, W., Zheng, S., Zhang, T., Guo, J., Manor, U.,
1111 Van Norman, J., et al. (2020). Auxin-induced signaling protein nanoclustering contributes to
1112 cell polarity formation. Nat. Commun. *11*, 1–14. 10.1038/s41467-020-17602-w.

1113 45. Marquès-Bueno, M.M., Armengot, L., Noack, L.C., Bareille, J., Rodriguez, L., Platre, M.P.,
1114 Bayle, V., Liu, M., Opdenacker, D., Vanneste, S., et al. (2021). Auxin-Regulated Reversible
1115 Inhibition of TMK1 Signaling by MAKR2 Modulates the Dynamics of Root Gravitropism.
1116 Curr. Biol. *31*, 228–237. 10.1016/J.CUB.2020.10.011.

1117 46. Dai, N., Wang, W., Patterson, S.E., and Bleecker, A.B. (2013). The TMK Subfamily of
1118 Receptor-Like Kinases in Arabidopsis Display an Essential Role in Growth and a Reduced
1119 Sensitivity to Auxin. PLoS One *8*, 60990. 10.1371/journal.pone.0060990.

1120 47. Chang, C., Eric Schaller, G., Patterson, S.E., Kwok, S.F., and Meyerowitz, E.M. (1992). The
1121 TMKl Gene from Arabidopsis Codes for a Protein with Structural and Biochemical
1122 Characteristics of a Receptor Protein Kinase. Plant Cell *4*, 1263–1271. 10.1105/tpc.4.10.1263.

1123 48. Oh, M.H., Wang, X., Kota, U., Goshe, M.B., Clouse, S.D., and Huber, S.C. (2009). Tyrosine
1124 phosphorylation of the BRI1 receptor kinase emerges as a component of brassinosteroid
1125 signaling in Arabidopsis. Proc. Natl. Acad. Sci. U. S. A. *106*, 658–663.
1126 10.1073/PNAS.0810249106.

1127 49. Wang, X., Goshe, M.B., Soderblom, E.J., Phinney, B.S., Kuchar, J.A., Li, J., Asami, T.,
1128 Yoshida, S., Huber, S.C., and Clouse, S.D. (2005). Identification and Functional Analysis of in
1129 Vivo Phosphorylation Sites of the Arabidopsis BRASSINOSTEROID-INSENSITIVE1
1130 Receptor Kinase. Plant Cell *17*, 1685–1703. 10.1105/TPC.105.031393.

1131 50. Paciorek, T., Zažímalová, E., Ruthardt, N., Petrášek, J., Stierhof, Y.D., Kleine-Vehn, J.,
1132 Morris, D.A., Emans, N., Jürgens, G., Geldner, N., et al. (2005). Auxin inhibits endocytosis
1133 and promotes its own efflux from cells. Nature *435*, 1251–1256. 10.1038/nature03633.

1134 51. Morffy, N., and Strader, L.C. (2022). Structural Aspects of Auxin Signaling. Cold Spring Harb.
1135 Perspect. Biol. *14*, a039883. 10.1101/cshperspect.a039883.

1136 52. Napier, R. (2021). The Story of Auxin-Binding Protein 1 (ABP1). Cold Spring Harb. Perspect.
1137 Biol. *13*, a039909. 10.1101/cshperspect.a039909.

1138 53. Er, E.E., Mendoza, M.C., Mackey, A.M., Rameh, L.E., and Blenis, J. (2013). AKT Facilitates
1139 EGFR Trafficking and Degradation by Phosphorylating and Activating PIKfyve. Sci. Signal. *6*,
1140 1–11. 10.1126/scisignal.2004015.

1141 54. Goh, L.K., and Sorkin, A. (2013). Endocytosis of Receptor Tyrosine Kinases. Cold Spring
1142 Harb. Perspect. Biol., a017459. 10.1101/cshperspect.a017459.

1143 55. Yu, Y., Tang, W., Lin, W., Zhou, X., Li, W., Li, Y., Chen, R., Cao, W., Perez-Henriquez, P.,
1144 Huang, R., et al. (2022). ABLs and TMKs are co-receptors for extracellular auxin. bioRxiv,
1145 2022.11.28.518138. https://doi.org/10.1101/2022.11.28.518138.

1146 56. Wang, J., Chang, M., Huang, R., Jiri, F., Yu, Y., Wen, M., Yang, Z., and Xu, T. (2022). Self-
1147 regulation of PIN1-driven auxin transport by cell surface-based auxin signaling in Arabidopsis.
1148 co-submitted to Cell.

1149 57. Wang, Y., Yan, X., Xu, M., Qi, W., Shi, C., Li, X., Ma, J., Tian, D., Shou, J., Wu, H., et al.
1150 (2022). TMK1-mediated auxin signal regulates membrane-associated clathrin in Arabidopsis
1151 roots. J. Integr. Plant Biol. 10.1111/jipb.13366.

1152 58. Brady, S.M., Orlando, D.A., Lee, J.Y., Wang, J.Y., Koch, J., Dinneny, J.R., Mace, D., Ohler,
1153 U., and Benfey, P.N. (2007). A high-resolution root spatiotemporal map reveals dominant
1154 expression patterns. Science *318*, 801–806. 10.1126/SCIENCE.1146265.

1155 59. Cao, M., Chen, R., Li, P., Yu, Y., Zheng, R., Ge, D., Zheng, W., Wang, X., Gu, Y., Gelová, Z.,
1156 et al. (2019). TMK1-mediated auxin signalling regulates differential growth of the apical hook.
1157 Nature *568*, 240–243. 10.1038/s41586-019-1069-7.

1158 60. Gao, Y., Zhang, Y., Zhang, D., Dai, X., Estelle, M., and Zhao, Y. (2015). Auxin binding
1159 protein 1 (ABP1) is not required for either auxin signaling or Arabidopsis development. Proc.
1160 Natl. Acad. Sci. U. S. A. *112*, 2275–2280. 10.1073/PNAS.1500365112.

1161 61. Gelová, Z., Gallei, M., Pernisová, M., Brunoud, G., Zhang, X., Glanc, M., Li, L., Michalko, J.,
1162 Pavlovičová, Z., Verstraeten, I., et al. (2021). Developmental roles of Auxin Binding Protein 1
1163 in Arabidopsis thaliana. Plant Sci. *303*, 110750. 10.1016/j.plantsci.2020.110750.

1164 62. Friml, J.J., Vieten, A., Sauer, M., Weijers, D., Schwarz, H., Hamann, T., Offringa, R., Jurgens,
1165 G., Cao, M., Chen, R., et al. (2003). Efflux-dependent auxin gradients establish the apical-basal
1166 axis of Arabidopsis. Nature *426*, 147–153. 10.1038/nature02085.

1167 63. Xu, J., and Scheres, B. (2005). Dissection of arabidopsis ADP-ribosylation factor 1 function in
1168 epidermal cell polarity. Plant Cell *17*, 525–536. 10.1105/tpc.104.028449.

1169 64. Jaillais, Y., Hothorn, M., Belkhadir, Y., Dabi, T., Nimchuk, Z.L., Meyerowitz, E.M., and

1170 Chory, J. (2011). Tyrosine phosphorylation controls brassinosteroid receptor activation by
1171 triggering membrane release of its kinase inhibitor. Genes Dev. *25*, 232–237.
1172 10.1101/gad.2001911.

1173 65. Simon, M.L.A., Platre, M.P., Assil, S., van Wijk, R., Chen, W.Y., Chory, J., Dreux, M.,
1174 Munnik, T., and Jaillais, Y. (2014). A multi-colour/multi-affinity marker set to visualize
1175 phosphoinositide dynamics in Arabidopsis. Plant J. *77*, 322–337. 10.1111/tpj.12358.

1176 66. Karimi, M., Depicker, A., and Hilson, P. (2007). Recombinational cloning with plant gateway
1177 vectors. Plant Physiol. *145*, 1144–1154. 10.1104/pp.107.106989.

1178 67. Lewis, D.R., and Muday, G.K. (2009). Measurement of auxin transport in Arabidopsis thaliana.
1179 Nat. Protoc. *4*, 437–451. 10.1038/nprot.2009.1.

1180 68. Grones, P., Abas, M., Hajný, J., Jones, A., Waidmann, S., Kleine-Vehn, J., and Friml, J.
1181 (2018). PID/WAG-mediated phosphorylation of the Arabidopsis PIN3 auxin transporter
1182 mediates polarity switches during gravitropism. Sci. Rep. *8*, 10279. 10.1038/s41598-018-
1183 28188-1.

1184 69. Czechowski, T., Stitt, M., Altmann, T., Udvardi, M.K., and Scheible, W.R. (2005). Genome-
1185 wide identification and testing of superior reference genes for transcript normalization in
1186 arabidopsis. Plant Physiol. *139*, 5–17. 10.1104/pp.105.063743.

1187 70. Grones, P., Chen, X., Simon, S., Kaufmann, W.A., De Rycke, R., Nodzyński, T., Zažímalová,
1188 E., and Friml, J. (2015). Auxin-binding pocket of ABP1 is crucial for its gain-of-function
1189 cellular and developmental roles. J. Exp. Bot. *66*, 5055–5065. 10.1093/jxb/erv177.

1190 71. Malamy, J.E., and Benfey, P.N. (1997). Organization and cell differentiation in lateral roots of
1191 Arabidopsis thaliana. Development *124*, 33–44. 10.1242/dev.124.1.33.

1192 72. von Wangenheim, D., Hauschild, R., Fendrych, M., Barone, V., Benková, E., and Friml, J.
1193 (2017). Live tracking of moving samples in confocal microscopy for vertically grown roots.
1194 Elife *6*. 10.7554/eLife.26792.

1195 73. Hayashi, Y., Nakamura, S., Takemiya, A., Takahashi, Y., Shimazaki, K., and Kinoshita, T.
1196 (2010). Biochemical Characterization of In Vitro Phosphorylation and Dephosphorylation of
1197 the Plasma Membrane H+-ATPase. Plant Cell Physiol. *51*, 1186–1196. 10.1093/pcp/pcq078.

1198 74. Tan, S., Abas, M., Verstraeten, I., Glanc, M., Molnár, G., Hajný, J., Lasák, P., Petřík, I.,
1199 Russinova, E., Petrášek, J., et al. (2020). Salicylic Acid Targets Protein Phosphatase 2A to
1200 Attenuate Growth in Plants. Curr. Biol. *30*, 381–395. 10.1016/j.cub.2019.11.058.

1201

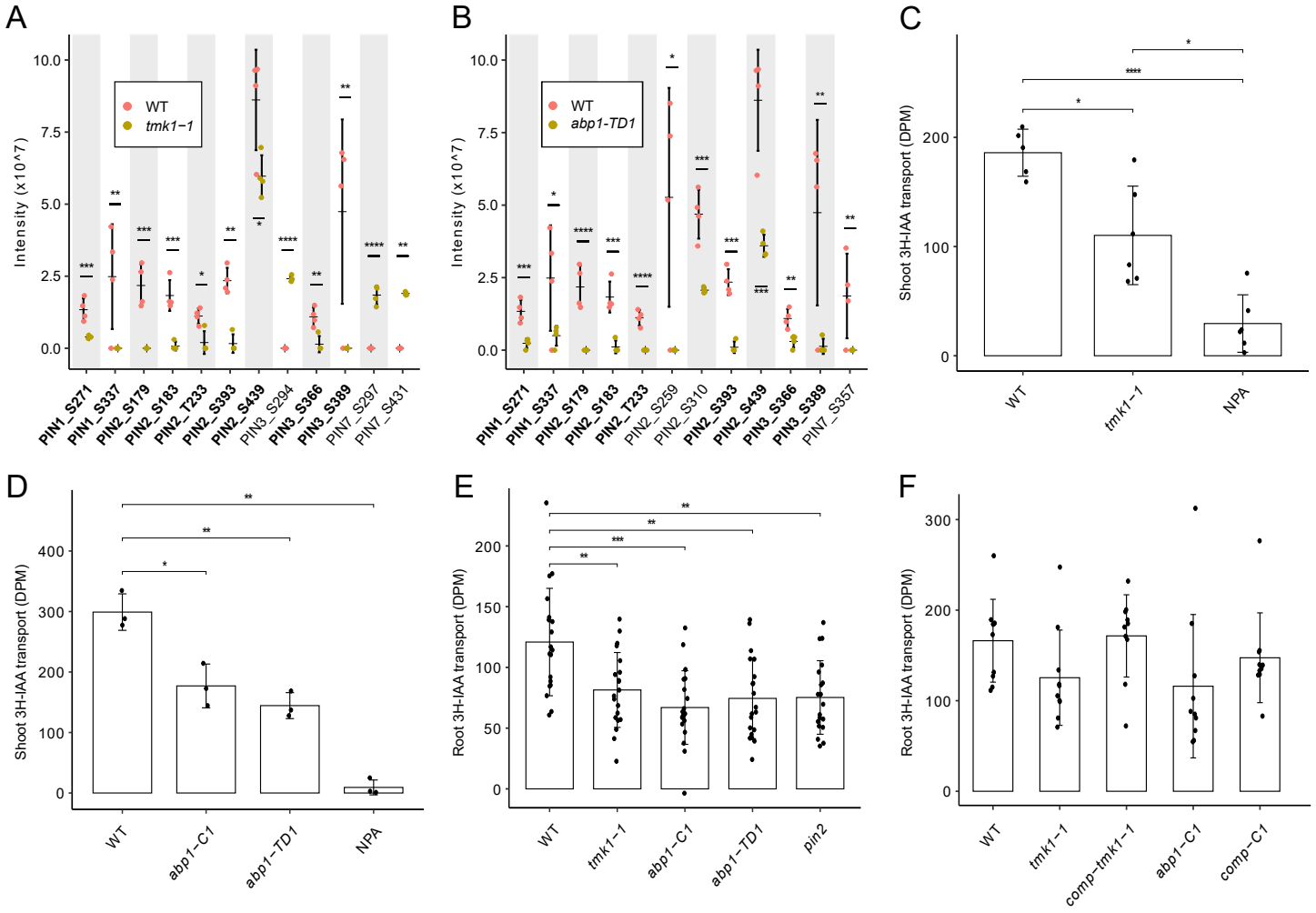
A
Intensity (x10^7)
WT
tmk1−1
PIN1_S271
PIN1_S337
PIN2_S179
PIN2_S183
PIN2_T233
PIN2_S393
PIN2_S439
PIN3_S294
PIN3_S366
PIN3_S389
PIN7_S297
PIN7_S431
B
Intensity (x10^7)
WT
abp1-TD1
PIN1_S271
PIN1_S337
PIN2_S179
PIN2_S183
PIN2_T233
PIN2_S259
PIN2_S310
PIN2_S393
PIN2_S439
PIN3_S366
PIN3_S389
PIN7_S357
C
Shoot 3H-IAA transport (DPM)
WT
tmk1−1
NPA
D
Shoot 3H-IAA transport (DPM)
WT
abp1−C1
abp1−TD1
NPA
E
Root 3H-IAA transport (DPM)
WT
tmk1−1
abp1−C1
abp1−TD1
pin2
F
Root 3H-IAA transport (DPM)
WT
tmk1−1
comp−tmk1−1
abp1−C1
comp−C1

Figure 1.

Figure 1. ABP1-TMK1 auxin perception targets PIN phosphorylation and polar auxin transport.

(A) Overview of PIN phospho-sites significantly regulated (FDR < 0.05) in *tmk1-1* mutant roots compared to WT after treatment with auxin (100 nM, 2 min). 4 independent biological replicates, mean ± SD, permutation-based t-tests with FDR-controlled p-values. Highlighted in bold are sites which are co-regulated in the *abp1-TD1* mutant. Data adapted from [15]. *p < 0.05, **p < 0.01, ***p < 0.001, ****p < 0.0001.

(B) Overview of PIN phospho-sites significantly regulated (FDR < 0.05) in *abp1-TD1* mutant roots compared to WT after treatment with auxin (100 nM, 2 min). 4 independent biological replicates, mean ± SD, permutation-based t-tests with FDR-controlled p-values. Highlighted in bold are sites which are co-regulated in the *tmk1-1* mutant. Data adapted from [15]. *p < 0.05, **p < 0.01, ***p < 0.001, ****p < 0.0001.

(C) Basipetal/rootward transport of radioactive ^{3}H-IAA in decapitated hypocotyls is defective in the *tmk1-1* mutant (genotype/treatment fixed effect: χ^2 = 60.64, df = 2, p = 6.78e-14). 10 µM NPA, an inhibitor of auxin transport, was used as a negative control. Pooled data from two independent experiments with similar results (repetition random effect: ΔAIC = 2.0, df = 1, p = 0.9999), mean ± SD. Asterisks show Holm-corrected unpaired two-sided t-tests. *p < 0.05, **p < 0.01, ***p < 0.001, ****p < 0.0001.

D) Basipetal/rootward transport of radioactive ^{3}H-IAA in decapitated hypocotyls is defective in *abp1* mutants (one-way ANOVA: $F_{3,8}$ = 60.13, p = 7.86e-06). 10 µM NPA, an inhibitor of auxin transport, was used as a negative control. Single experiment, n = 3 for each condition, mean ± SD. Asterisks show Holm-corrected unpaired two-sided t-tests. *p < 0.05, **p < 0.01, ***p < 0.001, ****p < 0.0001.

(E) Basipetal/shootward transport of radioactive ^{3}H-IAA in roots is defective in *tmk1-1* and *abp1* mutants (genotype/treatment fixed effect: χ^2 = 32.30, df = 4, p = 1.66e-06). Pooled data from two independent experiments with similar results (repetition random effect: ΔAIC = 1.1, df = 1, p = 0.0804), mean ± SD. Asterisks show Holm-corrected unpaired two-sided t-tests. *p < 0.05, **p < 0.01, ***p < 0.001, ****p < 0.0001.

(F) Complementation of defects in root basipetal/shootward transport of radioactive ^{3}H-IAA for the *TMK1::TMK1-FLAG/tmk1-1* (*comp-tmk1-1*) and *ABP1::GFP-ABP1/abp1-C1* (*comp-abp1-C1*) lines. Single experiment, n = 10 for each condition, mean ± SD.

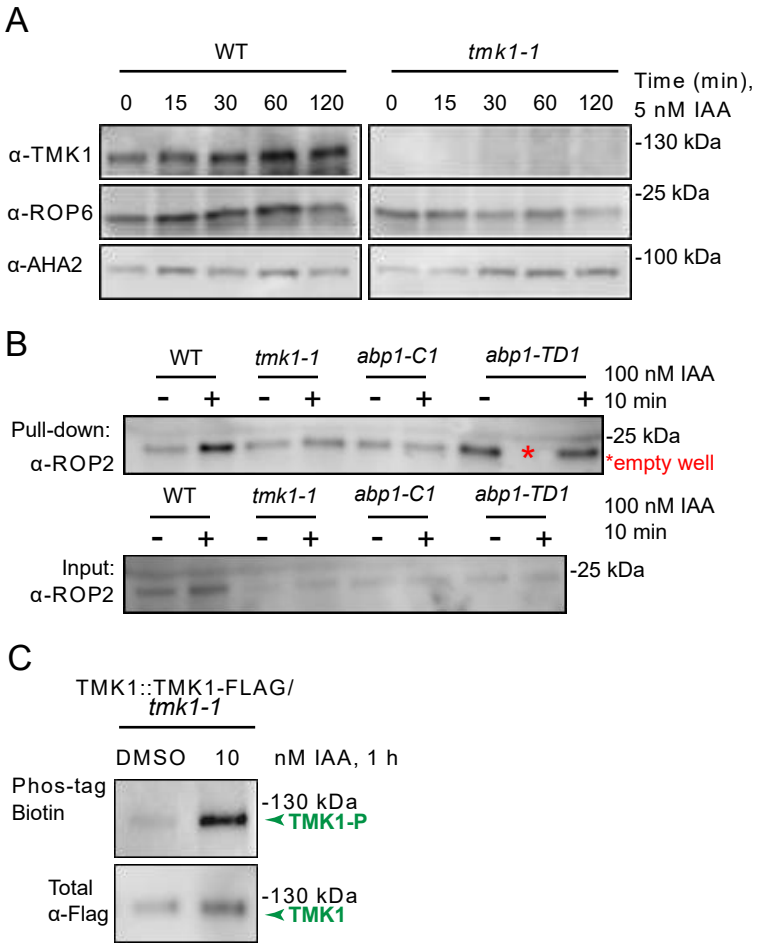
A
WT
tmk1-1
0 15 30 60 120
0 15 30 60 120
Time (min), 5 nM IAA
α-TMK1
α-ROP6
α-AHA2
-130 kDa
-25 kDa
-100 kDa
B
WT
tmk1-1
abp1-C1
abp1-TD1
100 nM IAA
10 min
Pull-down:
α-ROP2
-25 kDa
*empty well
Input:
α-ROP2
-25 kDa
C
TMK1::TMK1-FLAG/
tmk1-1
DMSO 10 nM IAA, 1 h
Phos-tag
Biotin
-130 kDa
TMK1-P
Total
α-Flag
-130 kDa
TMK1

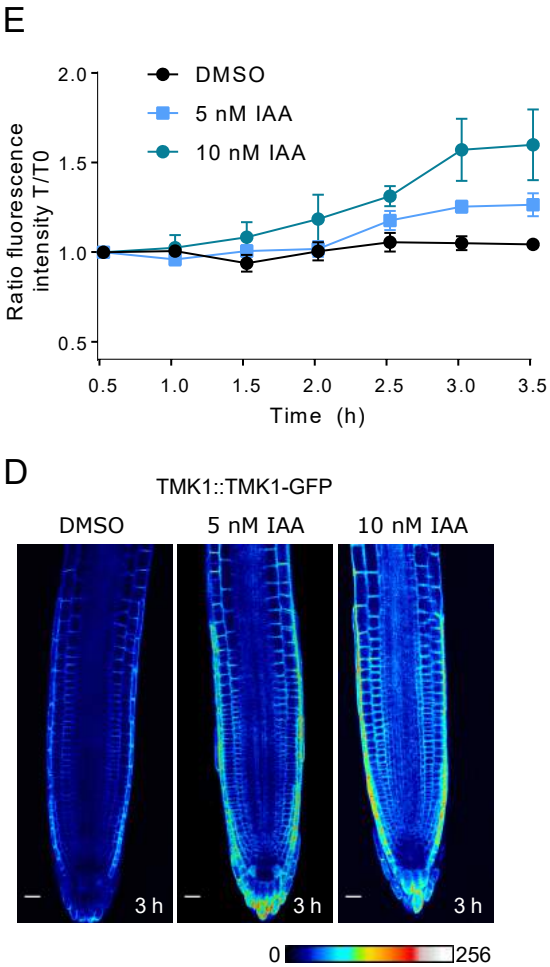
E
DMSO
5 nM IAA
10 nM IAA
Ratio fluorescence intensity T/T0
Time (h)
D
TMK1::TMK1-GFP
DMSO
5 nM IAA
10 nM IAA
3 h
0
256

Figure 2.

Figure 2. Auxin-induced activation of cell surface ABP1-TMK1 signalling in roots.

(A) Western Blot: time course of endogenous TMK1 and ROP6 protein levels in the microsomal fraction of 4-day-old WT and *tmk1-1* roots treated with 5 nM IAA (see Figure S2E for quantification). The experiment was repeated 3 times and representative data are shown. The loading control is reused in Figure 4A which depicts more data from the same experiment.

(B) Auxin-mediated activation of ROP signalling is defective in *tmk1-1* and *abp1* mutant backgrounds. Pull-down of active ROP GTPases from root protein extracts using a heterologously expressed GST-tagged CRIB domain from the RIC1 ROP effector. Both input and pull-down gels were blotted with an anti-ROP2 antibody.

(C) Comparison of TMK1-FLAG phosphorylation in untreated roots and roots treated with 10 nM IAA for 1h. Root *TMK1::TMK1-FLAG/tmk1-1* extracts treated with 10 nM IAA or DMSO control for 1 hour were used for immunoprecipitation with anti-Flag antibody. Phos-tag Biotin Probe was used to analyse TMK1 phosphorylation levels and anti-Flag antibody for total amount of immunoprecipitated TMK1-FLAG (see figure S2C for quantification).

(D) Representative intensity-coloured images of *TMK1::TMK1-GFP* expression in 4-day-old seedlings after a 3-hour treatment with 5 or 10 nM IAA. Scale bars represent 20 μm.

(E) Time-course quantification of *TMK1::TMK1-GFP* signal in root tips treated with IAA (5 or 10 nM) or DMSO control, normalized to the initial fluorescence value. Mean ± SD (n = 20; experiment repeated 3 times with representative data depicted).

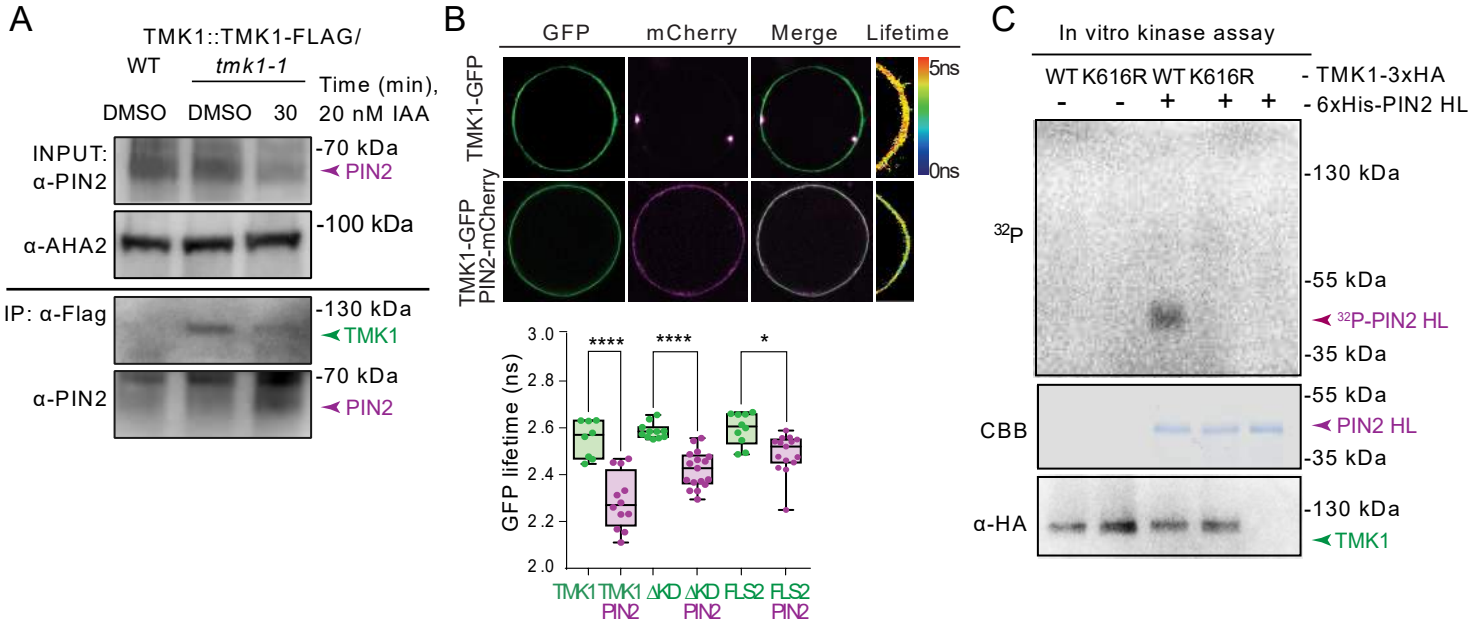
A
TMK1::TMK1-FLAG/
WT
tmk1-1
Time (min),
20 nM IAA
DMSO
DMSO
30
INPUT:
α-PIN2
-70 kDa
PIN2
α-AHA2
-100 kDa
IP: α-Flag
-130 kDa
TMK1
α-PIN2
-70 kDa
PIN2
B
GFP
mCherry
Merge
Lifetime
TMK1-GFP
TMK1-GFP
PIN2-mCherry
5ns
0ns
GFP lifetime (ns)
3.0
2.8
2.6
2.4
2.2
2.0
****
****
*
TMK1
TMK1 PIN2
ΔKD
ΔKD PIN2
FLS2
FLS2 PIN2
C
In vitro kinase assay
WT K616R WT K616R
- TMK1-3xHA
- 6xHis-PIN2 HL
32P
-130 kDa
-55 kDa
32P-PIN2 HL
-35 kDa
CBB
-55 kDa
PIN2 HL
-35 kDa
α-HA
-130 kDa
TMK1

Figure 3.

Figure 3. Auxin-mediated TMK1 interaction with and phosphorylation of PIN2.

(A) Auxin promotes the interaction between TMK1 and PIN2 in a co-immunoprecipitation (Co-IP) assay. Microsomal protein fraction from 20 nM IAA- or DMSO-treated roots expressing *TMK1::TMK1-FLAG/tmk1-1* was immunoprecipitated with an anti-FLAG antibody, and endogenous PIN2 was detected by blotting with an anti-PIN2 antibody. See Figure S3A for Co-IP with 5 nM IAA where input PIN2 abundance in the protein microsomal fraction is increased.

(B) FRET-FLIM analysis on transiently expressed *35S::TMK1-GFP*, *35S::TMK1$^{\Delta KD}$-GFP*, *35S::FLS2-GFP* and *35S::PIN2-mCherry* in root protoplasts. Fluorescence lifetime values are displayed as a heat map (for additional images see Figure S3B). Two-way ANOVA with post hoc tests (*$p < 0.05$; ****$p < 0.0001$).

(C) *In vitro* kinase assay showing that TMK1-3xHA directly phosphorylates the 6His-PIN2 hydrophilic loop (HL). Top panel, ^{32}P autoradiography; middle panel, CBB staining; bottom panel, immunoblot with an anti-HA antibody.

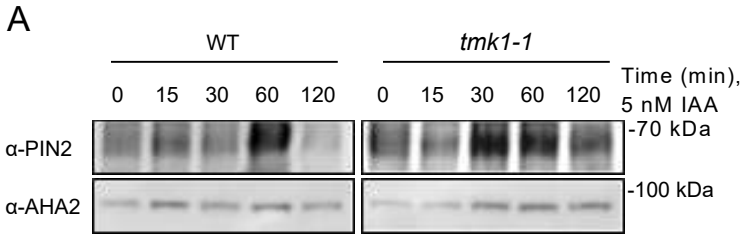
A
WT
tmk1-1
0 15 30 60 120
0 15 30 60 120
Time (min), 5 nM IAA
α-PIN2
α-AHA2
-70 kDa
-100 kDa

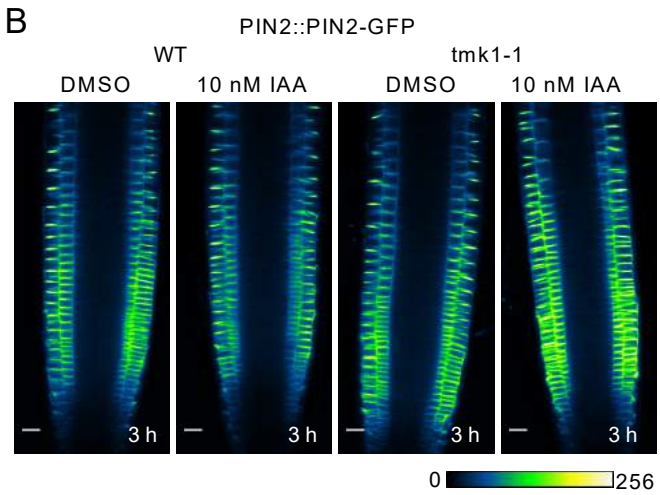
B
PIN2::PIN2-GFP
WT
tmk1-1
DMSO
10 nM IAA
DMSO
10 nM IAA
3 h
3 h
3 h
3 h
0
256

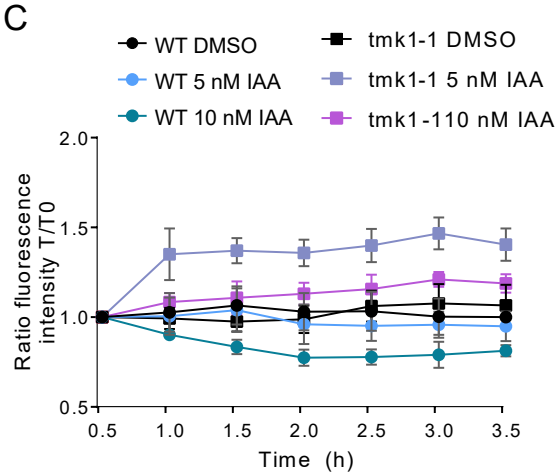
C
WT DMSO
WT 5 nM IAA
WT 10 nM IAA
tmk1-1 DMSO
tmk1-1 5 nM IAA
tmk1-110 nM IAA
Ratio fluorescence intensity T/T0
2.0
1.5
1.0
0.5
0.5 1.0 1.5 2.0 2.5 3.0 3.5
Time (h)

Figure 4.

Figure 4. TMK1 dynamically regulates root PIN2 levels in response to exogenous auxin.

(A) Western Blot: time course of endogenous PIN2 protein levels in the microsomal fraction of 4-day-old WT and *tmk1-1* roots treated with 5 nM IAA (see Figure S4A for quantification). The experiment was repeated 3 times and representative data are shown. The loading control (reused) and the anti-PIN2 immunoblot come from the same experiment as that shown in Figure 2A.

(B) Representative intensity coloured images of *PIN2::PIN2-GFP* after a 3-hour treatment with 10 nM IAA. Scale bars, 20 μm.

(C) Quantification of *PIN2::PIN2-GFP* in root tips of WT or *tmk1-1* seedlings treated with IAA (5, 10 nM or DMSO control), normalized to the initial fluorescence value. Mean ± SD (n = 20; experiment repeated 3 times with representative data depicted).

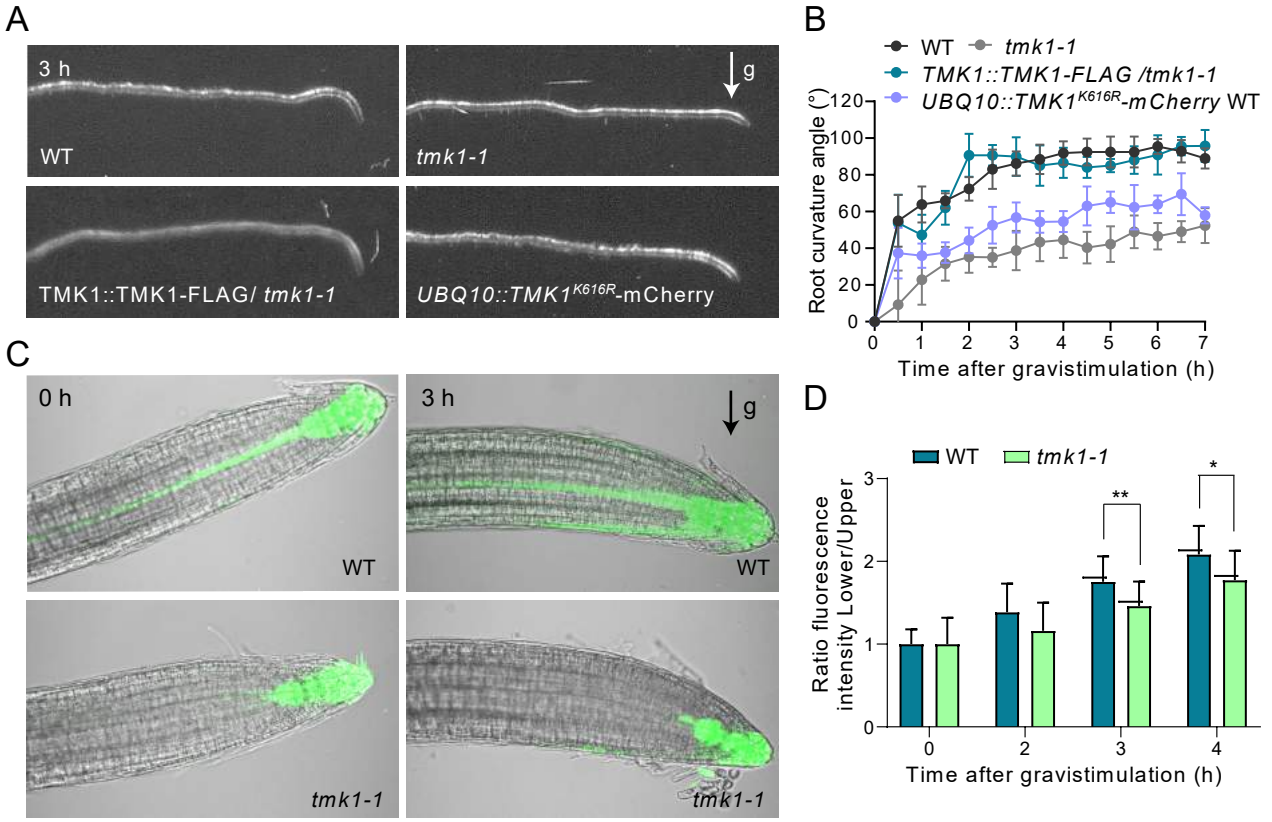
A
3 h
WT
g
tmk1-1
TMK1::TMK1-FLAG/ tmk1-1
UBQ10::TMK1K616R-mCherry
B
WT
tmk1-1
TMK1::TMK1-FLAG /tmk1-1
UBQ10::TMK1K616R-mCherry WT
Root curvature angle (°)
Time after gravistimulation (h)
C
0 h
3 h
g
WT
WT
tmk1-1
tmk1-1
D
WT
tmk1-1
Ratio fluorescence intensity Lower/Upper
Time after gravistimulation (h)
**
*

Figure 5.

Figure 5. TMK1 kinase activity is required for the gravitropic response.

(A) Representative images of root bending 3 hours after a 90° rotation for 4-day-old WT, mutant *tmk1-1*, kinase-dead *UBQ10::TMK1*^{K616R}*-mCherry*, and genetically complemented *TMK1::TMK1-FLAG/tmk1-1* seedlings.

(B) Time course of the gravitropic response for lines shown in (A) measured every 30 minutes, mean ± SD (n = 10; experiment repeated 3 times, a representative run is depicted). See Figure S5E for complete analysis and root growth rate data, and Table S2 for statistical analysis.

(C) Representative confocal images of asymmetric auxin response (visualized by *DR5rev::GFP*) at the lower side of the root before and after a 3-hour gravistimulation in WT and *tmk1-1* 4-day-old roots.

(D) Quantification of *DR5rev::GFP* asymmetry as a ratio of fluorescence intensity at the lower side to the upper side of gravistimulated roots at the indicated time points, normalized to the initial fluorescence value. Mean ± SEM of at least 3 independent experiments, n = 10. Two-way ANOVA with Dunnett's multiple comparison tests (*$p < 0.05$, **$p < 0.01$). 'g' represents the gravity vector.

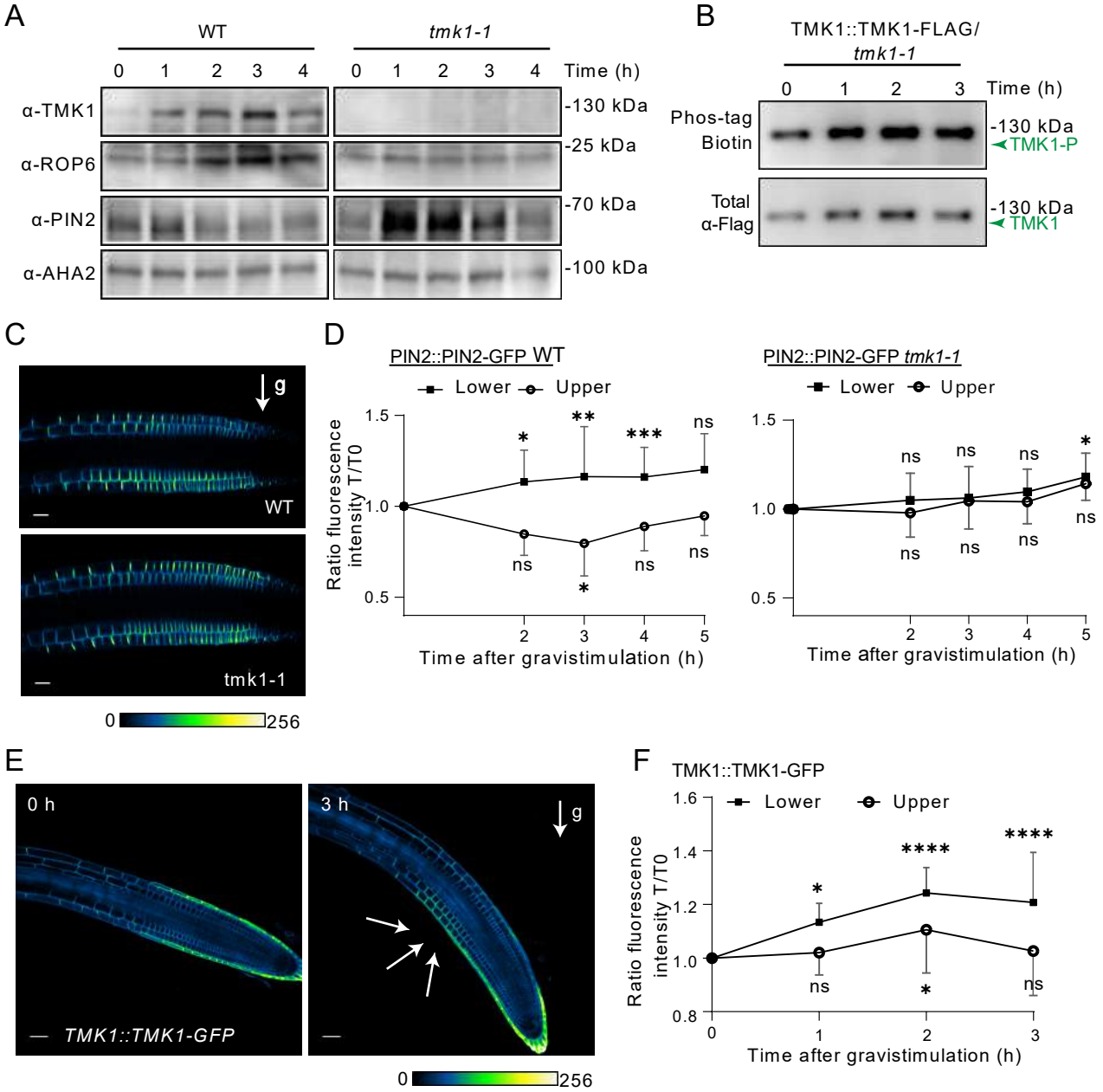
A
WT
tmk1-1
0 1 2 3 4 0 1 2 3 4 Time (h)
α-TMK1
α-ROP6
α-PIN2
α-AHA2
-130 kDa
-25 kDa
-70 kDa
-100 kDa
B
TMK1::TMK1-FLAG/
tmk1-1
0 1 2 3 Time (h)
Phos-tag
Biotin
Total
α-Flag
-130 kDa
TMK1-P
-130 kDa
TMK1
C
g
WT
tmk1-1
0
256
D
PIN2::PIN2-GFP WT
Lower
Upper
Ratio fluorescence intensity T/T0
Time after gravistimulation (h)
PIN2::PIN2-GFP tmk1-1
E
0 h
3 h
g
TMK1::TMK1-GFP
0
256
F
TMK1::TMK1-GFP
Lower
Upper
Ratio fluorescence intensity T/T0
Time after gravistimulation (h)

Figure 6.

Figure 6. TMK1 mediates PIN2 asymmetry during the root gravitropic response.

(A) Western Blot: time course of endogenous TMK1, ROP6 and PIN2 protein levels in the microsomal fraction of 4-day-old WT and *tmk1-1* roots after 0, 1, 2, 3 and 4 hours of gravistimulation. The experiment was repeated 3 times and representative data are shown. For quantification of protein levels see Figure S6C.

(B) TMK1-FLAG phosphorylation after gravistimulation. *TMK1::TMK1-FLAG/tmk1-1* was immunoprecipitated with an anti-FLAG antibody and detected using a Phos-tag Biotin Probe (see Figure S6D for quantification).

(C) Representative images of *PIN2::PIN2-GFP* in 4-day-old WT and *tmk1-1* seedlings after 4 hours of gravistimulation within a time course of 0, 2, 3, 4 and 5 hours of gravistimulation. 'g' represents the gravity vector. Scale bars, 20 µm.

(D) Quantification of PIN2-GFP ratio between the lower and upper sides of gravistimulated roots, normalized to the initial fluorescence value at the indicated time point. Mean ± SD (n = 8; experiment repeated 3 times with representative data depicted). Significant differences to timepoint 0 are shown by *p*-values, two-way ANOVA with Dunnett's post hoc tests (**** $p < 0.0001$).

(E) Intensity-coloured map of 4-day-old *TMK1::TMK1-GFP* root tips before and after 3 hours of a 90° gravitropic stimulus. White arrows indicate asymmetric TMK1-GFP distribution. Scale bars, 20 µm.

(F) Quantification of TMK1-GFP in the epidermis and cortex of the upper and lower root sides normalized to the initial fluorescence value, mean ± SD (n = 10). Experiment repeated 3 times with representative data depicted. Significant differences to timepoint 0 are shown by *p*-values, two-way ANOVA with Dunnett's post hoc tests (**** $p < 0.0001$).

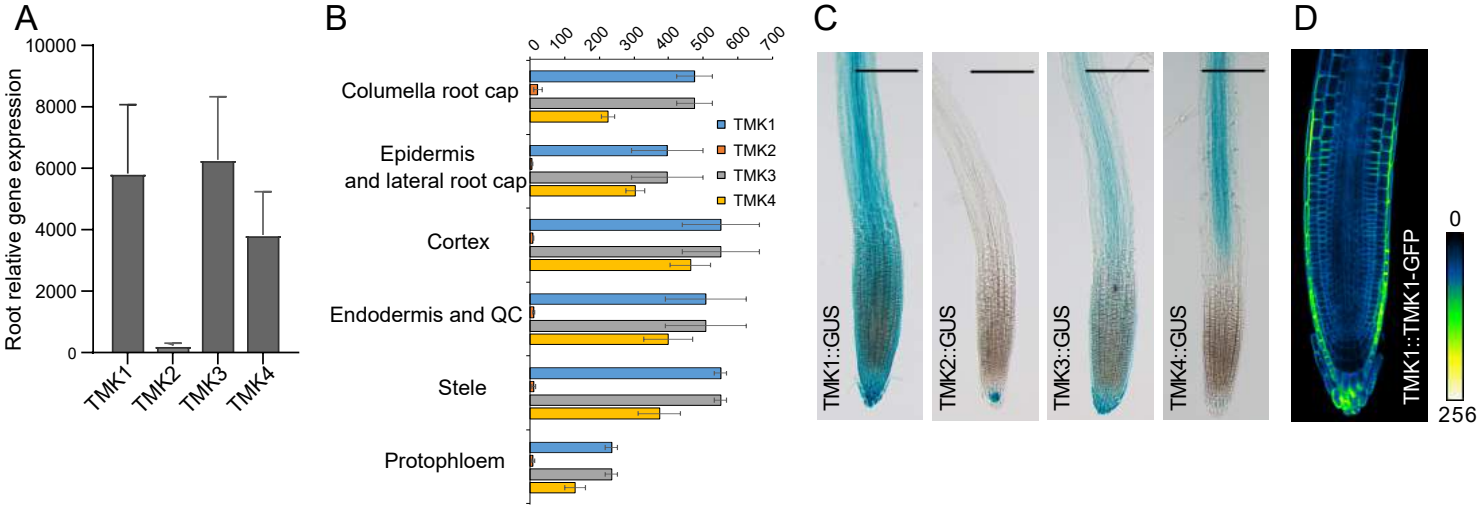
A
Root relative gene expression
10000
8000
6000
4000
2000
0
TMK1
TMK2
TMK3
TMK4
B
0
100
200
300
400
500
600
700
Columella root cap
Epidermis
and lateral root cap
Cortex
Endodermis and QC
Stele
Protophloem
TMK1
TMK2
TMK3
TMK4
C
TMK1::GUS
TMK2::GUS
TMK3::GUS
TMK4::GUS
D
TMK1::TMK1-GFP
0
256

Figure S1.

Figure S1. Expression of the TMK leucine-rich repeat receptor-like (LRR-RLK) kinase family in roots.

(A) Relative transcription levels of *TMK1*, *TMK2*, *TMK3* and *TMK4* in *Arabidopsis* roots from 803 samples assayed with the Affymetrix Arabidopsis ATH1 Genome Array. Data was obtained from the Genevestigator database (https://genevestigator.com). Mean ± SD.

(B) Relative expression levels of *TMK1*, *TMK2*, *TMK3* and *TMK4* in different root cell types obtained from high-resolution spatiotemporal microarray analysis of 5–6-day old roots reported in [58] (ePlant http://bar.utoronto.ca/eplant).

(C) Root tip expression pattern of *TMK1*, *TMK2*, *TMK3*, and *TMK4* promoters fused to the GUS transcriptional reporter. Scale bars, 100 μm.

(D) Representative intensity-colored image of *TMK1::TMK1-GFP* expression in 4-day-old root tips.

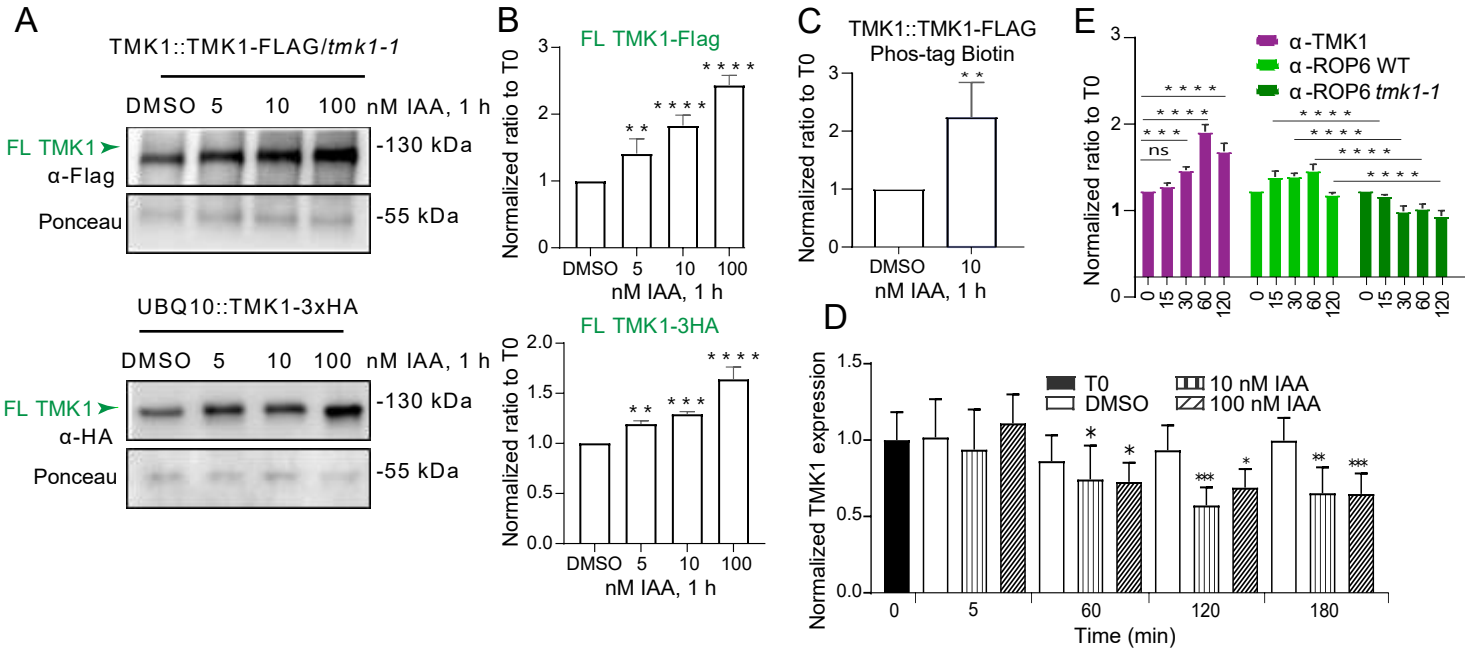
A
TMK1::TMK1-FLAG/tmk1-1
DMSO 5 10 100 nM IAA, 1 h
FL TMK1
α-Flag
-130 kDa
Ponceau
-55 kDa
UBQ10::TMK1-3xHA
DMSO 5 10 100 nM IAA, 1 h
FL TMK1
α-HA
-130 kDa
Ponceau
-55 kDa
B
FL TMK1-Flag
Normalized ratio to T0
DMSO 5 10 100
nM IAA, 1 h
FL TMK1-3HA
Normalized ratio to T0
DMSO 5 10 100
nM IAA, 1 h
C
TMK1::TMK1-FLAG
Phos-tag Biotin
Normalized ratio to T0
DMSO 10
nM IAA, 1 h
D
Normalized TMK1 expression
T0
DMSO
10 nM IAA
100 nM IAA
Time (min)
E
α-TMK1
α-ROP6 WT
α-ROP6 tmk1-1
Normalized ratio to T0
ns

Figure S2.

Figure S2. Auxin promotes TMK1 stability, phosphorylation state, and downstream signalling.

(A) Western blotting of total root protein extracts of 4-day-old *TMK1::TMK1-FLAG/tmk1-1* and *UBQ10::TMK1-3xHA* transgenic plants after 1-hour treatment with different concentrations of IAA (5, 10 and 100 nM IAA) or DMSO control. Ponceau staining was used as a loading control.

(B) Corresponding quantification of TMK1 protein levels normalized to Ponceau, and subsequently to DMSO condition, mean ±SD from 3 independent experiments. One-way ANOVA with Dunnett's multiple comparisons relative to DMSO (****$p<0.0001$).

(C) Quantification of TMK1-FLAG phosphorylated upon auxin treatment (10 nM, 1 hour) (see Figure 2C). Phosphorylation levels detected with a Phos-tag Biotin Probe were normalized to signal obtained from anti-FLAG detection, and subsequently to the initial value from time point 0. Mean ± SD of 3 independent biological replicates. *p*-value for comparison to DMSO was calculated with a two-tailed unpaired t-test (**$p < 0.01$).

(D) RT-qPCR time course of relative *TMK1* expression after 10 or 100 nM IAA treatment. Normalization was done to *PP2A* as a reference gene. The expression level at the start of the experiment (T0) was set to a relative value of 1 and statistical comparisons were made to this expression level (*$p < 0.05$, **$p < 0.01$ and ***$p < 0.001$).

(E) Time course of TMK1 and ROP6 protein levels in the membrane fraction of 4-day-old WT or *tmk1-1* roots upon auxin treatment (5 nM). Plasma membrane AHA2 H^+ ATPase (immunoblot shown in Figures 2A and 4A) was used as a loading control. We then normalized to initial protein levels at time point 0. Values are mean ± SD from 3 independent experiments. Two-way ANOVA with Dunnett's multiple comparisons (****$p < 0.0001$).

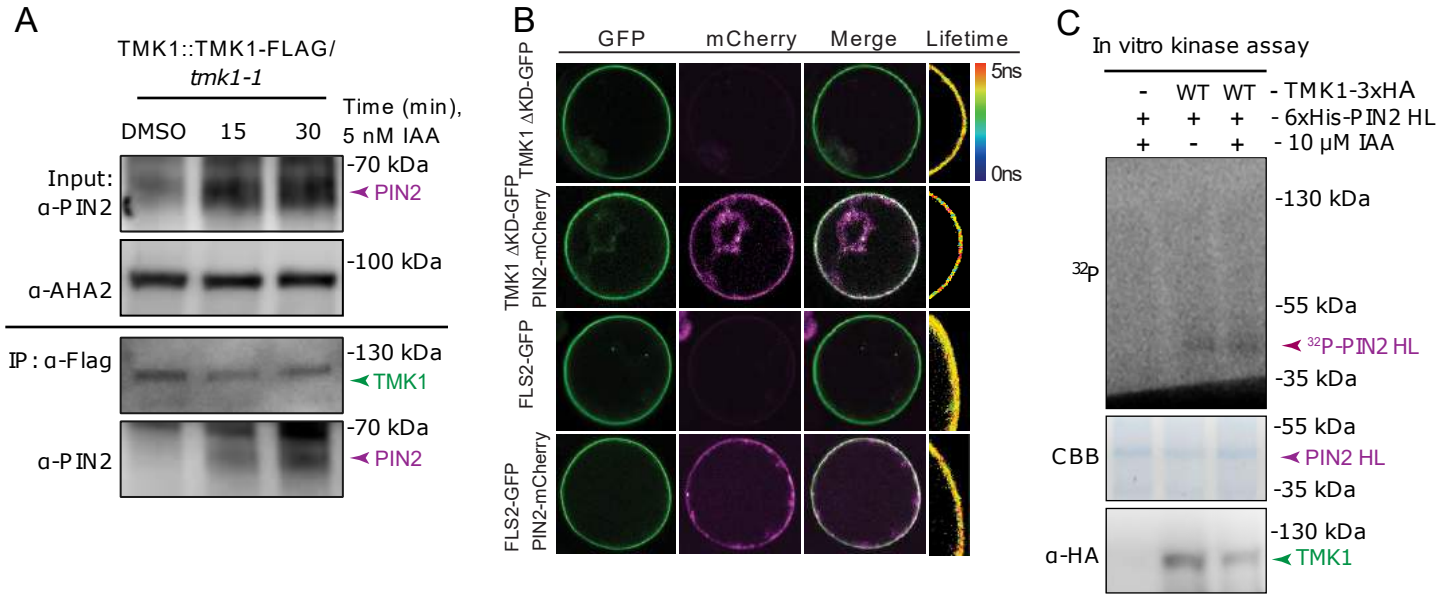
A
TMK1::TMK1-FLAG/
tmk1-1
DMSO
15
30
Time (min),
5 nM IAA
Input:
α-PIN2
-70 kDa
PIN2
α-AHA2
-100 kDa
IP : α-Flag
-130 kDa
TMK1
α-PIN2
-70 kDa
PIN2
B
GFP
mCherry
Merge
Lifetime
5ns
0ns
TMK1 ΔKD-GFP
TMK1 ΔKD-GFP
PIN2-mCherry
FLS2-GFP
FLS2-GFP
PIN2-mCherry
C
In vitro kinase assay
- WT WT - TMK1-3xHA
+ + + - 6xHis-PIN2 HL
+ - + - 10 μM IAA
32P
-130 kDa
-55 kDa
32P-PIN2 HL
-35 kDa
CBB
-55 kDa
PIN2 HL
-35 kDa
α-HA
-130 kDa
TMK1

Figure S3.

Figure S3. TMK1 interacts with PIN2 in an auxin-dependent manner and phosphorylates it.

(A) Co-IP assay showing the interaction of TMK1 with PIN2 upon low auxin treatment (5 nM IAA). Microsomal protein fraction from WT was used as a control for unspecific binding of endogenous PIN2 (shown in Figure 3A, same experiment).

(B) FRET-FLIM analysis on transiently expressed *35S::TMK1$^{\Delta KD}$-GFP, 35S::TMK1$^{\Delta KD}$-GFP/35S::PIN2-mCherry, 35S::FLS2-GFP* and *35S::FLS2-GFP/35S::PIN2-mCherry* in root protoplasts (the same experiment is shown in Figure 3B). GFP fluorescence lifetime was calculated as described in the Methods section. The heat map depicts fluorescence lifetime values (see Figure 3B for lifetime analysis).

(C) *In vitro* kinase assay showing phosphorylation of the 6His-PIN2 HL substrate by TMK1-3xHA in the presence or absence of auxin. Top panel, ^{32}P-autoradiography; middle panel, CBB staining; bottom panel, immunoblot with an anti-HA antibody.

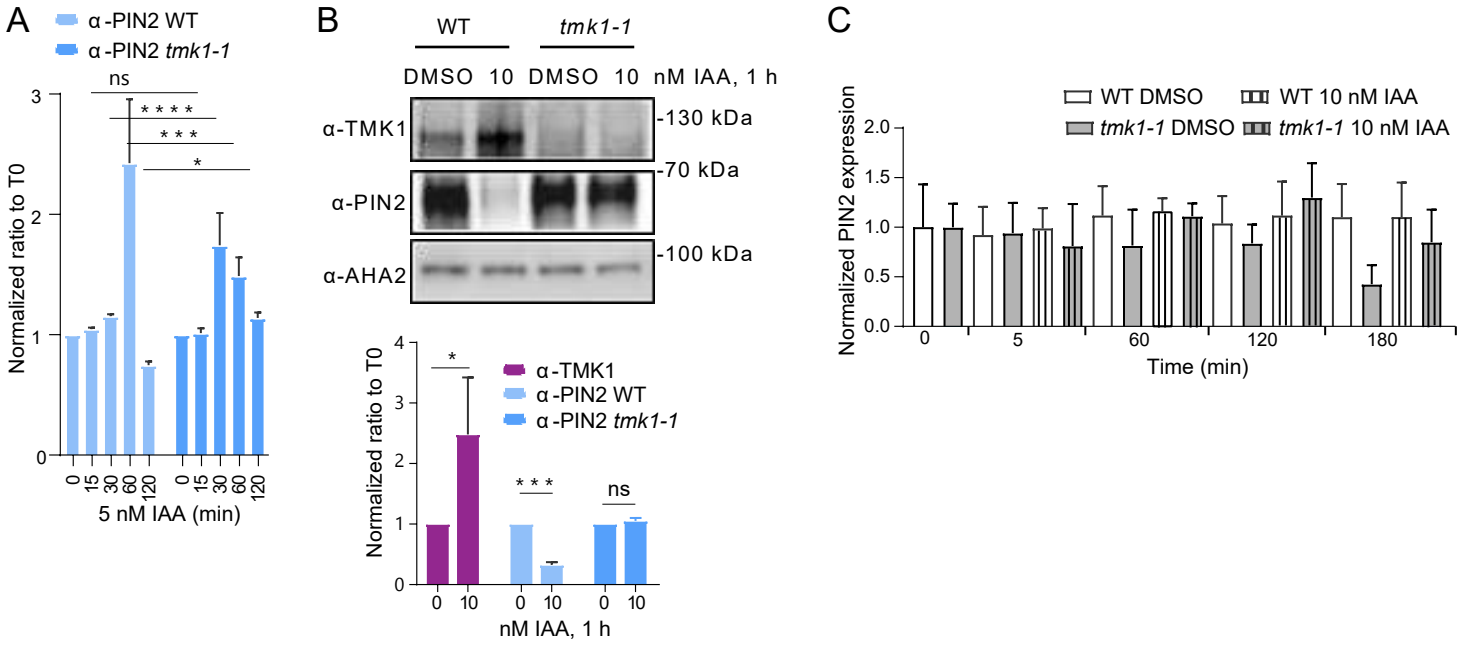
A
α-PIN2 WT
α-PIN2 tmk1-1
ns
****
***
*
Normalized ratio to T0
0
15
30
60
120
5 nM IAA (min)
B
WT
tmk1-1
DMSO 10 DMSO 10 nM IAA, 1 h
α-TMK1
α-PIN2
α-AHA2
-130 kDa
-70 kDa
-100 kDa
α-TMK1
α-PIN2 WT
α-PIN2 tmk1-1
nM IAA, 1 h
C
WT DMSO
WT 10 nM IAA
tmk1-1 DMSO
tmk1-1 10 nM IAA
Normalized PIN2 expression
Time (min)

Figure S4.

Figure S4. TMK1 regulates PIN2 stability on the post-transcriptional level.

(A) Time course of PIN2 protein levels in the membrane fraction of 4-day-old WT or *tmk1-1* roots upon auxin treatment (5 nM). Plasma membrane AHA2 H^+-ATPase (immunoblot shown in Figures 2A and 4A) was used as a loading control. We then normalized to initial protein levels at time point 0. Values are mean ± SD from 3 independent experiments. Two-way ANOVA with Dunnett's multiple comparisons (****$p < 0.0001$).

(B) Left panel: immunoblot of endogenous TMK1 and PIN2 in the microsomal fraction in response to 1-hour treatment with 10 nM IAA in WT versus *tmk1-1* roots. Right panel: quantification of protein levels detected with anti-TMK1 and anti-PIN2 antibodies normalized to the loading control, and then to DMSO. Values are mean ± SD from 3 independent experiments. Two-way ANOVA with Dunnett's multiple comparisons (****$p<0.0001$).

(C) Comparison of PIN2 expression in WT versus *tmk1-1* upon auxin treatment. Relative expression of PIN2 upon 10 and 100 nM IAA treatment at different time points (0, 5, 60, 120 and 180 minutes). Normalization was done to *PP2A* as a reference gene. The expression level at the start of the experiment was set to the relative value of 1.

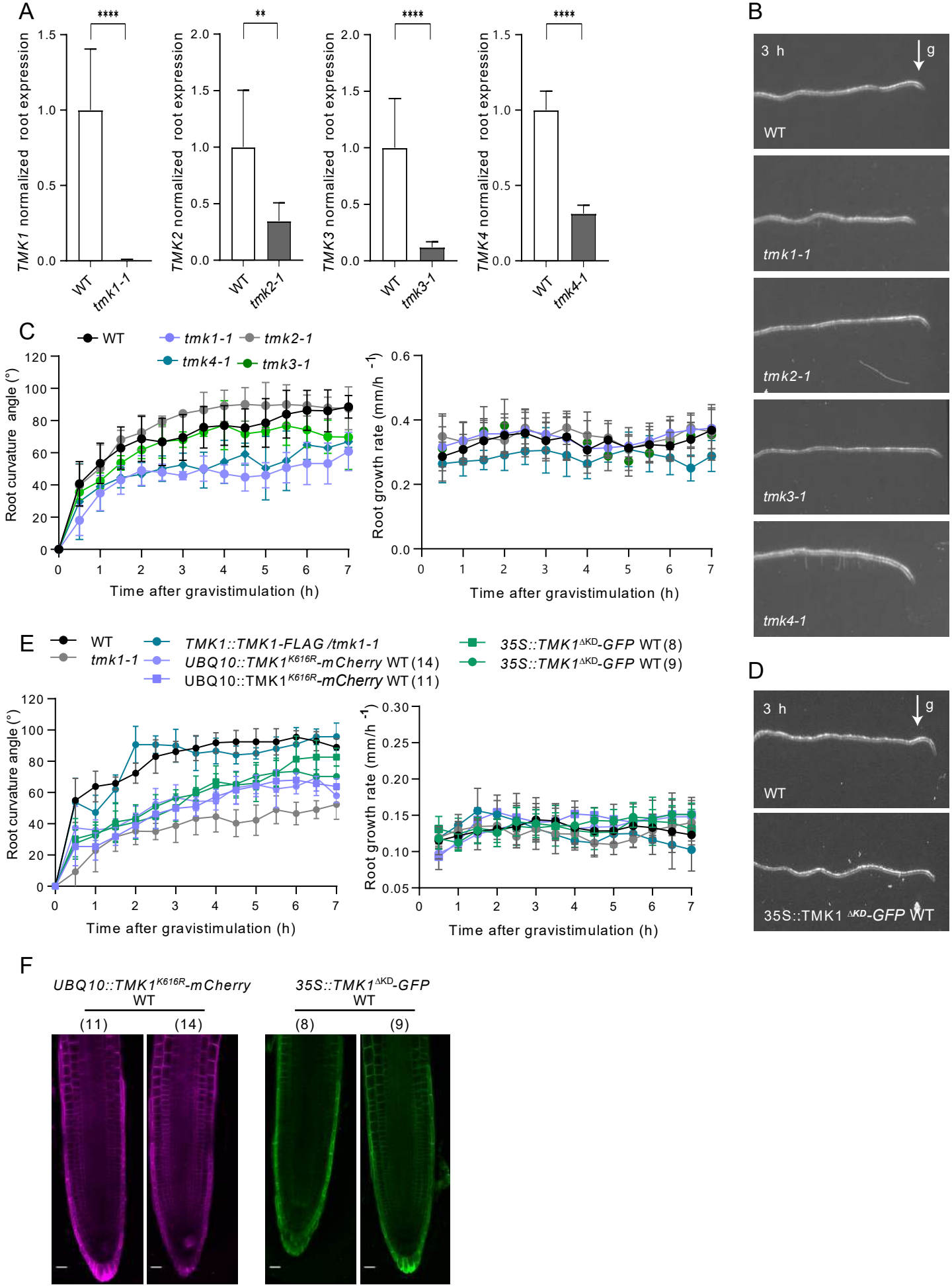
A
****
**
****
****
TMK1 normalized root expression
TMK2 normalized root expression
TMK3 normalized root expression
TMK4 normalized root expression
WT
tmk1-1
tmk2-1
tmk3-1
tmk4-1
B
3 h
g
WT
tmk1-1
tmk2-1
tmk3-1
tmk4-1
C
WT
tmk1-1
tmk2-1
tmk4-1
tmk3-1
Root curvature angle (°)
Root growth rate (mm/h -1)
Time after gravistimulation (h)
D
3 h
g
WT
35S::TMK1 ΔKD-GFP WT
E
WT
tmk1-1
TMK1::TMK1-FLAG /tmk1-1
UBQ10::TMK1K616R-mCherry WT (14)
UBQ10::TMK1K616R-mCherry WT (11)
35S::TMK1ΔKD-GFP WT (8)
35S::TMK1ΔKD-GFP WT (9)
Root curvature angle (°)
Root growth rate (mm/h -1)
Time after gravistimulation (h)
F
UBQ10::TMK1K616R-mCherry
WT
(11)
(14)
35S::TMK1ΔKD-GFP
WT
(8)
(9)

Figure S5.

Figure S5. *TMK* genes are required for robust gravitropic root bending.

(A) Expression levels of *TMK1, TMK2, TMK3* and *TMK4* determined by RT-qPCR in root samples of 4-day-old WT and *tmk1-1, tmk2-1, tmk3-1* and *tmk4-1* seedlings. RNA was extracted in 4 independent biological repeats and the RT-qPCR analysis was performed in 3 technical repetitions. Expression levels were normalized against the expression level of PP2A as a housekeeping gene. Asterisks indicate significantly lower expression levels in the respective mutants, two-tailed unpaired t-tests (****$p < 0.0001$ and **$p < 0.01$).

(B) Root gravitropism in single mutants of TMK family genes. Root curvature angles were measured every 30 min after reorientation by a 90° rotation. Representative images of 4-day-old WT, *tmk1-1, tmk2-1, tmk3-1,* and *tmk4-1* single mutant roots after 3 hours of reorientation.

(C) Time course of root tip angle changes and root growth rates, mean ± SEM from 3 independent experiments (n= 30-40). See Table S1 for statistical analysis.

(D) Representative images of root bending 3 hours after a 90° rotation of 4-day-old WT and the overexpression line of TMK1 without a cytoplasmic kinase domain (*35S::TMK1$^{\Delta KD}$-GFP*).

(E) Time course of the gravitropic response including *35S::TMK1$^{\Delta KD}$-GFP* lines and root growth rate from the same experiment at the indicated time points, mean ± SD (n = 10; experiment repeated 3 times with representative data depicted).

(F) Representative images of primary roots expressing the *UBQ10::TMK1^{K616R}-mCherry* and *35S::TMK1$^{\Delta KD}$-GFP* constructs.

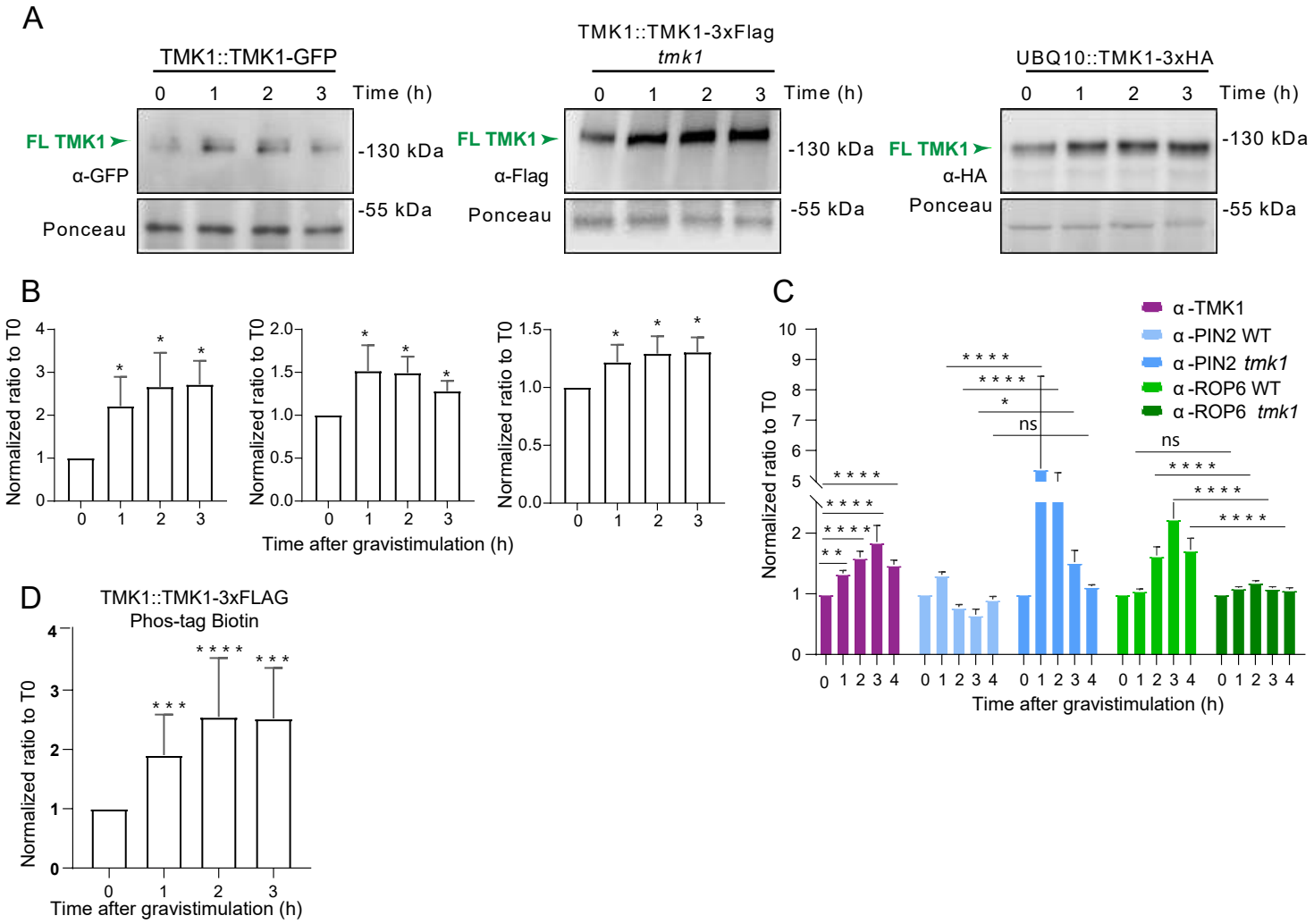
A
TMK1::TMK1-GFP
TMK1::TMK1-3xFlag
tmk1
UBQ10::TMK1-3xHA
0 1 2 3 Time (h)
FL TMK1
α-GFP
α-Flag
α-HA
Ponceau
-130 kDa
-55 kDa
B
Normalized ratio to T0
Time after gravistimulation (h)
C
α-TMK1
α-PIN2 WT
α-PIN2 tmk1
α-ROP6 WT
α-ROP6 tmk1
ns
D
TMK1::TMK1-3xFLAG
Phos-tag Biotin

Figure S6.

Figure S6. Gravistimulation promotes TMK1 stability, phosphorylation state, and downstream signalling

(A) Western blotting of total root protein extracts of 4-day-old *TMK1::TMK1-GFP, TMK1::TMK1-FLAG/tmk1-1* and *UBQ10::TMK1-3xHA* transgenic plants after 0, 1, 2, 3h of gravistimulation. Ponceau staining was used as a loading control.

(B) Corresponding quantification of the relative TMK1 protein levels normalized first to Ponceau, and then to initial protein levels at time point 0, values are mean ± SD from 3 independent experiments. One-way ANOVA with Dunnett's multiple comparisons to timepoint 0 (****$p < 0.0001$).

(C) Comparison of TMK1, PIN2, and ROP6 endogenous levels in the membrane fraction during gravistimulation of WT and *tmk1-1* 4-day-old roots. Normalization was to plasma membrane AHA2 ATPase (immunoblot analysis shown in Figure 6A), and then to initial protein levels at timepoint 0. Values are mean ± SD from 3 independent experiments. Two-way ANOVA with Dunnett's multiple comparisons to timepoint 0 (****$p < 0.0001$).

(D) Quantification of phosphorylated TMK1 levels during gravistimulation (see Figure 6B). TMK1 protein levels detected with biotinylated Phos-tag Probe were normalized to the signal obtained from anti-FLAG detection, and then to the initial value from timepoint 0. Values are mean ± SD from 3 experiments with 3 independent biological replicates. Two-way ANOVA with Dunnett's multiple comparisons to timepoint 0 (****$p < 0.0001$).